Redox Biology 59 (2023) 102582

Contents lists available at ScienceDirect

Redox Biology

journal homepage: www.elsevier.com/locate/redox

Microbiota-induced lipid peroxidation impairs obeticholic acid-mediated antifibrotic effect towards nonalcoholic steatohepatitis in mice

Aoxiang Zhuge [a,1], Shengjie Li [a,1], Yin Yuan [a,1], Shengyi Han [a], Jiafeng Xia [a], Qiangqiang Wang [a], Shuting Wang [a], Pengcheng Lou [a], Bo Li [a,b,**], Lanjuan Li [a,b,c,*]

[a] State Key Laboratory for Diagnosis and Treatment of Infectious Diseases, National Clinical Research Center for Infectious Diseases, National Medical Center for Infectious Diseases, Collaborative Innovation Center for Diagnosis and Treatment of Infectious Diseases, The First Affiliated Hospital, Zhejiang University School of Medicine, Hangzhou, 310003, China

[b] Research Units of Infectious Disease and Microecology, Chinese Academy of Medical Sciences, Beijing, 100730, China

[c] Jinan Microecological Biomedicine Shandong Laboratory, Jinan, 250000, China

A B S T R A C T

Obeticholic acid (OCA) has been examined to treat non-alcoholic steatohepatitis (NASH), but has unsatisfactory antifibrotic effect and deficient responsive rate in recent phase III clinical trial. Using a prolonged western diet-feeding murine NASH model, we show that OCA-shaped gut microbiota induces lipid peroxidation and impairs its anti-fibrotic effect. Mechanically, *Bacteroides* enriched by OCA deconjugates tauro-conjugated bile acids to generate excessive chenodeoxycholic acid (CDCA), resulting in liver ROS accumulation. We further elucidate that OCA reduces triglycerides containing polyunsaturated fatty acid (PUFA-TGs) levels, whereas elevates free PUFAs and phosphatidylethanolamines containing PUFA (PUFA-PEs), which are susceptible to be oxidized to lipid peroxides (notably arachidonic acid (ARA)-derived 12-HHTrE), inducing hepatocyte ferroptosis and activating hepatic stellate cells (HSCs). Inhibiting lipid peroxidation with pentoxifylline (PTX) rescues anti-fibrotic effect of OCA, suggesting combination of OCA and lipid peroxidation inhibitor could be a potential antifibrotic pharmacological approach in clinical NASH-fibrosis.

1. Introduction

Farnesoid X receptor (FXR, encoded by *NR1H4*), a bile acid (BA) ligand-triggered transcriptional factor, has been reported to function in metabolic homeostasis, exemplified by liver regeneration as well as glucose, lipid and cholesterol metabolism [1–4]. OCA is a semisynthetic FXR agonist derived from chenodeoxycholic acid (CDCA) with much higher affinity than natural BA ligands [5]. To date, OCA has been developed for treating various chronic liver disorders, including biliary atresia, primary biliary cholangitis (PBC), non-alcoholic fatty liver disease (NAFLD), non-alcoholic steatohepatitis (NASH), and primary sclerosing cholangitis (PBS), and was approved for the clinical second-line treatment of PBC by the FDA in 2016 [6–8]. However, a recent phase III clinical trial of OCA for NASH with fibrosis demonstrated that OCA exhibited moderate anti-fibrotic effect and deficient responsive rate (18% on 10 mg dose and 23% on 25 mg dose, compared to 12% of placebo) [9,10]. Additionally, OCA cannot ameliorate PBC-induced liver fibrosis and may exacerbate biliary injury in obstructive cholestasis [11,12]. Moreover, OCA has been reported to reduce the mitochondrial function of hepatocytes and promote cell apoptosis [13,14]. FDA rejected to support accelerated approval of OCA for the treatment of NASH due to multiple adverse events observed in clinical trials, including dose-dependent pruritus, increase of LDL cholesterol and risk of gallstone formation, as well as rare deterioration liver function [8,9,15,16]. Thus, there raises an essential issue that which driver in NASH progression impairs anti-fibrotic effect of OCA, which may have important clinical significance to improve its responsive rate.

Hepatic fibrosis is primarily resulted from activation of hepatic stellate cells (HSCs), in which process HSCs are transited from a quiescent vitamin A-rich cell to one that is fibrogenic, proliferative, and proinflammatory [17]. HSCs are mainly activated by hepatocyte-derived and inflammatory cell-derived fibrogenic signals, and lipotoxic response to hepatocellular injury contributes to release of ROS, which in turn stimulates fibrogenic expression of HSCs [18,19]. Primarily, regulated cell death (RCD) in metabolic liver disease is comprised of apoptosis, necroptosis, pyroptosis and ferroptosis [20,21]. Among these types of death, ferroptosis, which linking lipid metabolism, redox state and iron balance, has been recognized as major type of RCD

* Corresponding author. Research Units of Infectious Disease and Microecology, Chinese Academy of Medical Sciences, Beijing, 100730, China.
** Corresponding author. Research Units of Infectious Disease and Microecology, Chinese Academy of Medical Sciences, Beijing, 100730, China.
E-mail addresses: suon@zju.edu.cn (B. Li), ljli@zju.edu.cn (L. Li).
[1] Aoxiang Zhuge, Shengjie Li and Yin Yuan contributed equally to this study.

https://doi.org/10.1016/j.redox.2022.102582
Received 6 November 2022; Received in revised form 15 December 2022; Accepted 19 December 2022
Available online 22 December 2022
2213-2317/© 2022 The Authors. Published by Elsevier B.V. This is an open access article under the CC BY-NC-ND license (http://creativecommons.org/licenses/by-nc-nd/4.0/).

to initiate cell death and inflammation in NASH [22]. Further, hepatic iron overload and abnormal deposition have been detected in approximately one-third of NAFLD patients, which is regarded as one of the critical factors to induce NASH and subsequent fibrosis [20,22–24]. Nevertheless, the specific mechanism and key driver of ferroptosis in NASH need further exploitation and whether OCA can alleviate ferroptosis remains unknown.

In this study, we investigated whether OCA could alleviate various pathological alternations of NAFLD, and verified the role of OCA-derived microbiome and lipidome in its unsatisfactory *anti*-ferroptotic and anti-fibrotic effect. We verified OCA-shaped gut microbiota induced ROS accumulation, for *Helicobacter* was related with gut peroxidation state, and *Bacteroides* could elevate liver ROS levels through generating CDCA. Moreover, OCA reduced hepatic levels of triglycerides containing polyunsaturated fatty acids (PUFA-TGs), whereas increased free PUFAs and phosphatidylethanolamine-anchored arachidonic acids (ARA-PEs), which triggered lipid peroxidation and subsequent ferroptosis. Mechanistically, ARA-derived lipid peroxide, notably 12-HHTrE, was accumulated and contributed to hepatocyte ferroptosis, which in turn activated HSCs and ultimately impaired the anti-fibrotic effect of OCA. These results tap a potential therapeutic approach to liver fibrosis through combining OCA with lipid peroxidation inhibitors. Importantly, we demonstrate that OCA synergized with pentoxifylline (PTX) additively alleviate OCA-unresponsive liver fibrosis in NASH mice.

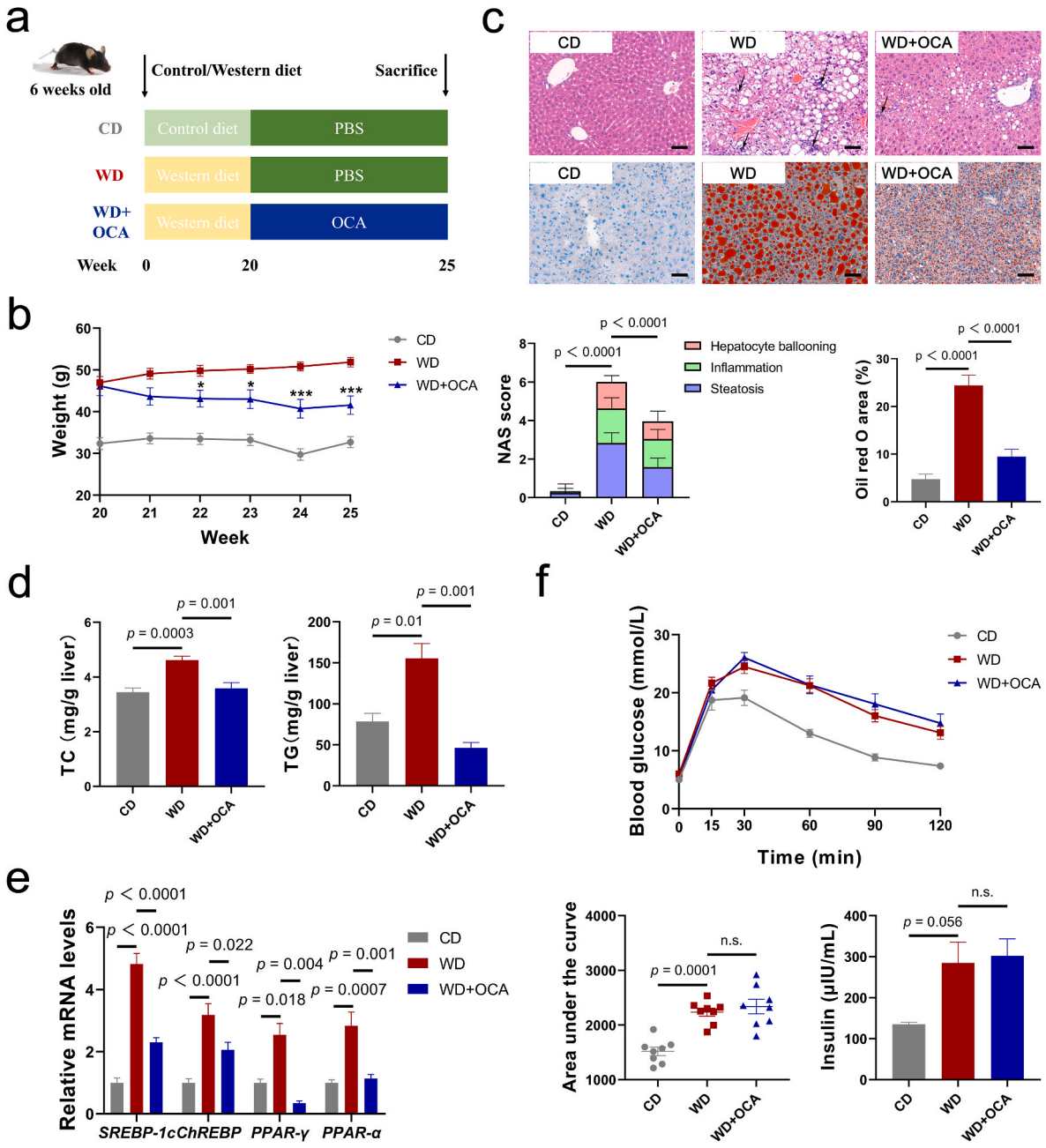

Fig. 1. OCA ameliorates hepatic lipid accumulation but exhibits limit impact on insulin resistance. (a) Experimental design. (b) Body mass change after OCA administration (n = 8 per group). (c) Representative images of liver sections stained with HE and Oil red O (upper channel) and corresponding NAS score and Oil red O area index (n = 8 per group) (lower channel), scale bar 80 μm. Arrows indicate inflammatory cell infiltration in the liver. (d) Levels of TC and TG in the liver (n = 7–8 per group). (e) Liver expressions of lipid metabolism gene *SREBP-1c*, *ChREBP*, *PPAR-γ* and *PPAR-α* (n = 6 per group). (f) Intravenous glucose tolerance test (IGTT), area under the curve (AUC) and serum insulin levels (n = 7–8 per group). Data are presented as mean ± SEM. (For interpretation of the references to color in this figure legend, the reader is referred to the Web version of this article.)

2. Results

2.1. OCA ameliorated hepatic lipid accumulation and inflammation

FXR agonist, notably OCA, has been proved to ameliorate key components of NASH activity including impaired glucose and lipid homeostasis as well as inflammasome activation [25–27]. However, there are lack of systematic studies to conclude specific impacts of OCA on NASH profiles. To address this concern, the effects of OCA on NASH were evaluated in WD-fed mice (Fig. 1a). In line with the previous studies, OCA significantly reduced body mass and relieved hepatic lipid accumulation, presenting as lowered NAS score and Oil red O (ORO) area based on HE and ORO staining (Fig. 1b and c). Compared with the WD-fed mice, mice administrated with OCA exhibited decreased total cholesterol (TC) and TG levels in the liver and serum (Fig. 1d, Fig. S1a) and increased ratio of HDL to VLDL and LDL (Fig. S1b), while free fatty acid (FFA) remained unchanged. Consistently, hepatic mRNA levels of lipid metabolism genes *SREBP-1c*, *ChREBP*, *PPAR-γ* and *PPAR-α* further indicated that OCA elicited activation of lipogenesis that is motivated by WD (Fig. 1e).

Insulin resistance was proved to interact with glucose and lipid metabolism and contribute to fibrosis in NASH [18,28]. Previous studies demonstrated contradictory findings about whether OCA alleviates insulin resistance [26,29,30]. To elucidate interrelationship between OCA treatment and insulin resistance, intraperitoneal glucose tolerance test (IGTT) was employed, which indicated no difference in glucose tolerance and serum insulin levels (Fig. 1f). Conversely, serum GLP-1 and PPY levels exhibited uptrends (Fig. S1d).

We further investigated inflammatory activity, which participates in NASH progression. OCA-treated mice were characterized with normalized serum ALT and AST levels and improved neutrophil infiltration compared with WD-fed mice (Fig. 2a and b). Consistently, systemic inflammation was ameliorated by OCA treatment, characterized by reduced levels of IL-1β, IL-3, IL-5, IL-6 and elevated anti-inflammatory cytokine IL-10 (Fig. 2c). Similar results were observed in the hepatic mRNA expressions of inflammatory genes *IL-1β*, *IL-6*, *IL-18*, *TNF-α*, *MCP-1* and *CXCL2* (Fig. 2d).

These findings indicated that OCA reversed WD-induced lipid

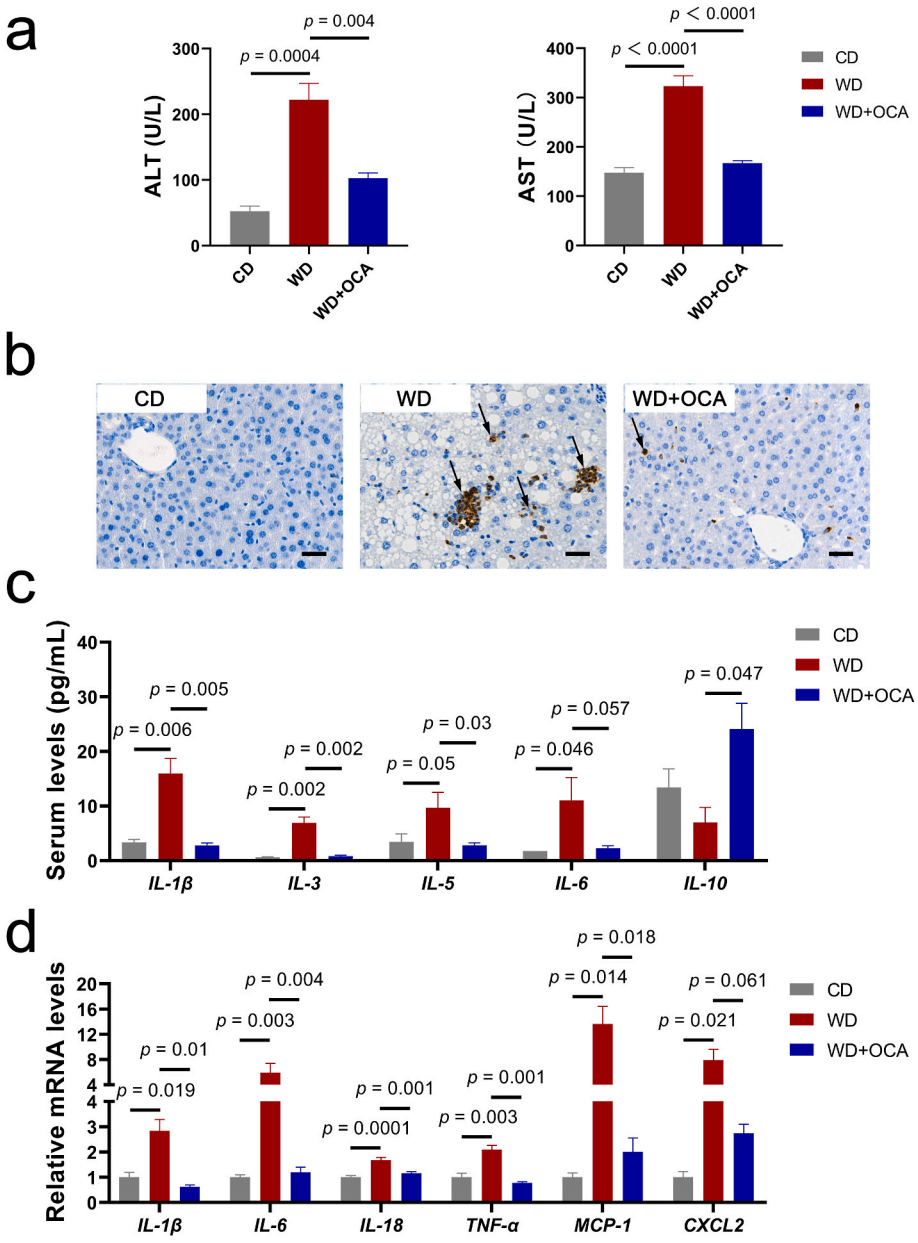

Fig. 2. OCA alleviates hepatic and systemic inflammation. (a) Serum ALT and AST levels (n = 8 per group). (b) Representative images of liver sections with MPO immunohistochemistry staining, scale bar 40 μm. Arrows indicate neutrophil infiltration in the liver. (c) Serum concentrations of inflammatory cytokines IL-1β, IL-3, IL-5, IL-6 and IL-10 (n = 8 per group). (d) Liver expressions of inflammatory genes *IL-1β*, *IL-6*, *IL-18*, *TNF-α*, *MCP-1* and *CXCL2* (n = 6 per group). Data are presented as mean ± SEM.

accumulation and inflammation, whereas had limited effects on insulin resistance.

2.2. OCA exerted limited anti-oxidative and anti-fibrotic effects

Oxidative stress has been recognized as a key driver in development of NASH-related fibrosis [31,32]. To identify whether OCA modulates oxidative stress status in the NASH, levels of reactive oxygen species (ROS) were assessed. Dihydroethidium (DHE) staining revealed no significant alternations in the hepatic ROS concentrations (Fig. 3a and d). Consistent with histological analysis, oxidative genes *NOX2* and *MPO*, anti-oxidative genes *GSTM1* and *CAT*, and peroxidation indexes GSH, MDA and SOD activity also exhibited no difference (Fig. 3c and d). Likewise, OCA is not effective in decreasing WD-induced ileum ROS levels (Figs. S2a and b) and normalizing serum levels of anti-oxidants (Fig. S2c).

Previous researches on various animal models as well as in a phase III clinical study demonstrated that OCA exhibits dose-dependent and modest anti-fibrotic effect [9,33–36]. Thus, we further evaluated the anti-fibrotic effects of OCA on WD-fed mice. Sirius red and α-SMA staining presented no difference upon OCA treatment (Fig. 3a and b), and expressions of fibrotic genes *ACTA2* and *TGF-β1* were not significantly reduced (Fig. 3c).

These results demonstrated that OCA was not effective in modulating oxidative stress and lipid peroxidation, which we supposed may contribute to its inadequate anti-fibrotic effects.

2.3. OCA modulated bile acid metabolism to induce liver lipid peroxidation

Accumulated bile acids in the liver and blood are associated with hepatocyte apoptosis, oxidative damage and HSC activation [36–38]. Thus, we verified the effect of OCA on FXR signal and BA homeostasis. As predicted, OCA notably reduced serum and fecal total BAs levels (Fig. 4a). In detail, conjugated and secondary BAs were enriched in the serum; unconjugated BAs were presented as declined CA, LCA and DCA and elevated CDCA, α-MCA, β-MCA and UDCA (Fig. 4b and c, Fig. S3a). Similarly, fecal BAs spectrum was characterized as decreased CA, CDCA, HDCA and DCA (Fig. 4c). Primarily, taurine-conjugated BAs rather than glycine-conjugated BAs were reduced upon OCA treatment (Fig. S3b). Consistent with BA profiles, signals in hepatic and ileum FXR axis (*FXR*, *SHP*, *BSEP* and *FGF15*) were up-regulated and elevated BA synthetic enzymes (*CYP7A1*, *CYP27A1*, *CYP7B1* and *CYP8B1*) induced by WD were reversed upon OCA treatment (Fig. 4d and e). Interestingly, BA synthetic enzymes in the classic pathway (*CYP7A1*, *CYP8B1*) exhibited greater reduction compared to those in the alternative pathway (*CYP27A1*, *CYP7B1*) (Fig. 4d and e). We further investigated whether accumulated CDCA could induce oxidative damage. We found CDCA dose-dependently induced ROS accumulation in the mitochondria of the human hepatocyte cell lines L-02 and elevated MDA levels (Fig. 4f and g). These results strongly supported that OCA-enriched CDCA could induce liver ROS accumulation and lipid peroxidation.

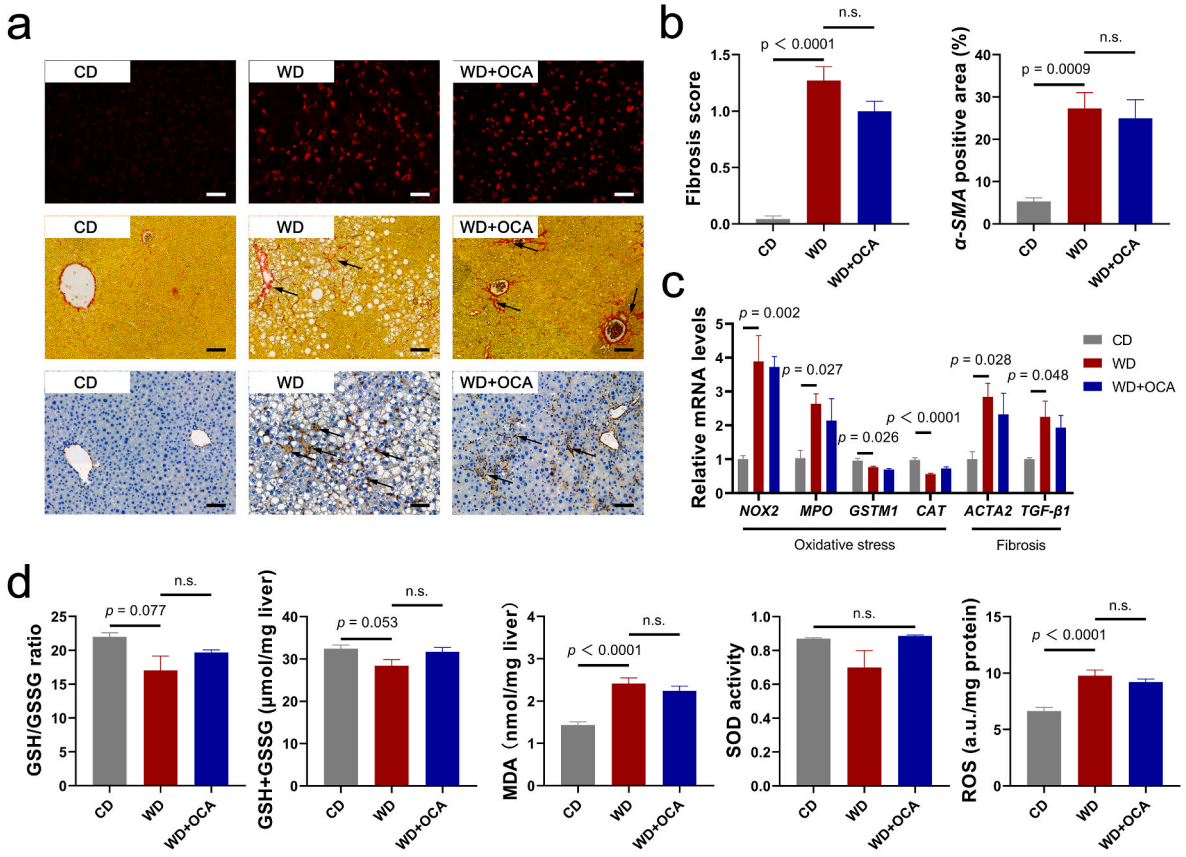

Fig. 3. OCA exerts limited anti-oxidative and anti-fibrotic effects. (a) Representative images of liver sections with dihydroethidium (DHE) (scale bar 40 μm), Sirius Red and α-SMA (scale bar 80 μm) immunohistochemistry staining. Arrows indicate collagen fibers and α-SMA expressions in the liver. (b) Fibrosis score based on Sirius Red staining according to NAS scoring system and α-SMA positive area (n = 8 per group). (c) Liver expressions of oxidative-damage-related genes *NOX2*, *MPO*, *GSTM1* and *CAT*, and fibrosis-related genes *ACTA2* and *TGF-β1* (n = 6 per group). (d) Hepatic concentrations of oxidative stress biomarkers GSH, MDA, SOD and ROS (n = 8 per group). Data are presented as mean ± SEM. (For interpretation of the references to color in this figure legend, the reader is referred to the Web version of this article.)

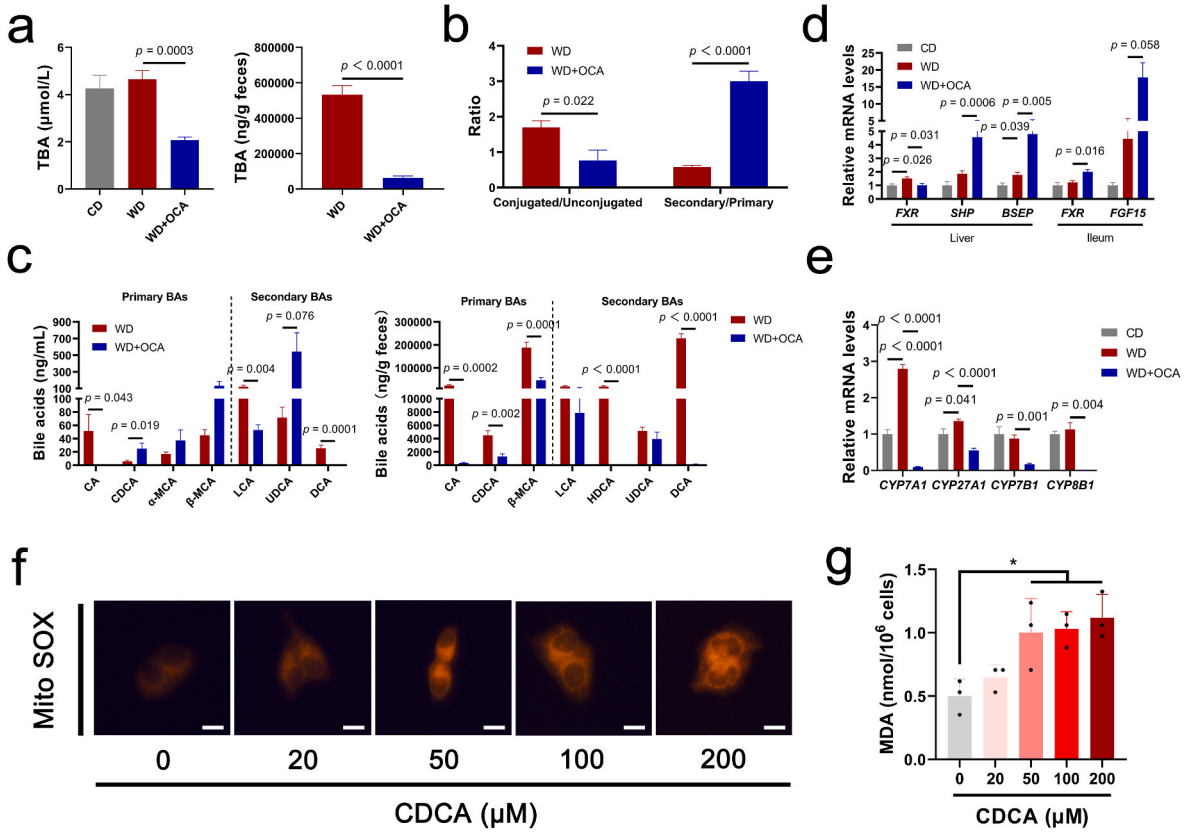

Fig. 4. OCA-derived CDCA induces mitochondrial ROS accumulation. (a) Total bile acid (TBA) levels in the serum and stool (n = 7–8 per group). (b) Compositions of BA in the serum (n = 7–8 per group). (c) BA profiles in the serum and stool (n = 7–8 per group). (d) Expression of FXR signals and its target genes *SHP*, *BSEP* and *FGF15* (n = 6 per group). (e) Hepatic mRNA expression levels of BA synthetic enzymes *CYP7A1*, *CYP27A1*, *CYP7B1* and *CYP8B1* (n = 6 per group). Mitochondrial ROS detected by Mito-Tracker Red CMXRos (red, scale bar 10 μm) (f) and MDA levels (g) in the human hepatocyte cell line L-02 treated with different concentrations of CDCA (n = 3 per group). Data are presented as mean ± SEM. *$p < 0.05$. (For interpretation of the references to color in this figure legend, the reader is referred to the Web version of this article.)

2.4. *OCA-shaped gut microbiota was associated with lipid peroxidation*

Crosstalk between the gut epithelia and some commensal bacteria induces the generation of ROS, which participates in NASH progression [39–41]. Considering OCA targets intestine, we hypothesized that OCA mediates alternations in gut microbiota, which contributes to lipid peroxidation. To this end, 16S rRNA sequencing was conducted focused on the stool and mucosa-related microbiome. OCA obviously elevated microbial richness (Chao1, Shannon) impaired by WD intervention and mediated shifts in community compositions (Fig. 5a and b, Figs. S4a and b). These alternations included an increase in phylum *Bacteroidota* and decreases in *Desulfobacterota* and *Fimicutes* (Fig. 5c). Further, enriched family *Helicobacteraceae* and depleted *Lachnospiraceae* were detected in the OCA-treated group (Fig. 5c and d). Similarly, LEfSe revealed that OCA-derived microbiome was characterized as oxidative stress corresponding taxa *Bacteroides* and *Rikenellaceae* under phylum *Bacteroidota* along with genus *Helicobacter* (Fig. 5e, Figs. S4c and d). Subsequent correlation analysis revealed significant positive association between liver ROS levels and *Bacteroides* enrichment, and *Helicobacter* enrichment was positive related with ileum ROS levels (Fig. 5f). To further elucidate the role of the gut microbiota in lipid peroxidation, we conducted intestinal decontamination in OCA-tread mice to remove gut microbes, and found OCA remarkably reduced WD-induced ROS accumulation and MDA levels in the presence of antibiotics (ABX) (Fig. 5g and h, Fig. S4e). We also tested the bile salt hydrolase (BSH) activity of OCA-shaped microbiota to generate CDCA, and found BSH activity elevated by OCA was abolished upon ABX co-treatment (Fig. 5i). Together, these results indicated that the effect of OCA on lipid peroxidation was, at least partially, influenced through altering the gut microbiota. *Bacteroides* and *Helicobacter* were two oxidative-corresponding microbes related with liver and gut ROS accumulation, respectively.

2.5. *OCA selectively mediated hepatic lipid profiles susceptible to lipid peroxidation*

OCA has been reported to regulate TG (main component of lipid droplet) synthesis and intestinal absorption of lipids dependent of FXR pathway [42]. However, the impact of OCA on hepatic lipid profiles has not been extensively characterized. Thus, we utilized UPLC-ESI-MS/MS to detect OCA-modified lipid classes in the liver and filtered 1788 individual lipid species. As predicted, OCA mediated selective changes in hepatic lipid profiles, characterized by reduced TG and ceramides phosphate (CerP) classes as well as elevated PE, dimethylphosphatidylethanolamine (dMePE), fatty acid (FA), ceramides (Cer) and sphingomyelin (SM) classes (Fig. 6a). Further identification of key lipid species revealed that OCA reduced majority of TGs containing fatty acid with two or more double bonds (PUFA) (Fig. 6b). Conversely, free ω-3 PUFAs doco-sahexaenoic acid (DHA), docosa-pentaenoic acid (DPA) and ω-6 PUFAs linoleic acid (LA) and ARA were detected to concentrate after OCA treatment (Fig. 6c and d). KEGG analysis also revealed that OCA up-regulated metabolism of PUFAs, predominantly ARA (20:4 ω-6), LA (18:2 ω-6) and alpha-linolenic acid (ALA, 18:3 ω-3) (Fig. 6e). Notably, compared to the reduction of ARA-TGs and unchanged free ARA, ARA-containing glycerophospholipid PEs (ARA-PEs) were significantly elevated by OCA treatment (Fig. 6f), while other glycerophospholipids

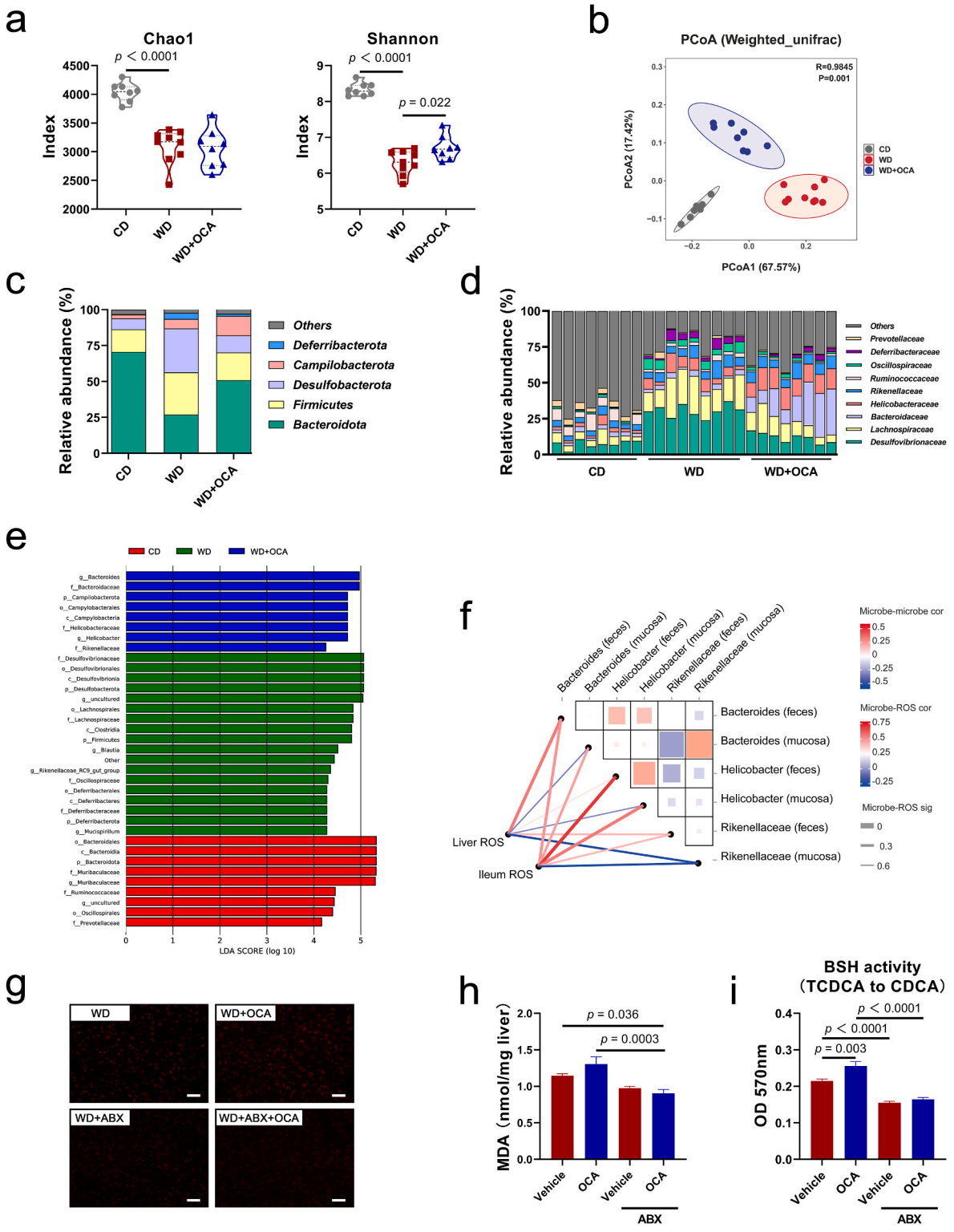

Fig. 5. OCA-shaped gut microbiota induces lipid peroxidation. (a) α-diversity indexes Chao1 and Shannon (n = 8–9 per group). (b) PCoA analysis based on Weighted UniFrac distance (n = 8–9 per group). Relative abundance at the phylum (c) and family (d) level (n = 8–9 per group). (e) Linear discriminant analysis (LDA) Effect Size (LEfSe) related LDA score of differential taxa. Only the taxa whose LDA score > 4 is displayed. (f) Correlation heatmap between ROS levels and gut microbial taxa based on the Spearman analysis. Color key and square size indicates the strength of correlation between microbes (r value). Color key (r value) and line width (*p* value) indicates the strength of correlation between microbe and ROS levels. Dark red indicates a more positive correlation; dark blue indicates a more negative correlation; white indicates no correlation. Thicker line indicates a more significant difference. (g) Representative images of liver sections with DHE staining in mice treated with OCA with or without antibiotics, scale bar 40 μm. (h) Hepatic MDA levels in mice treated with OCA with or without antibiotics (n = 8 per group). (i) Gut microbial BSH activity analyzed by ninhydrin assay (TCDCA to CDCA) (n = 8 per group). Data are presented as mean ± SEM. ABX, antibiotics. (For interpretation of the references to color in this figure legend, the reader is referred to the Web version of this article.)

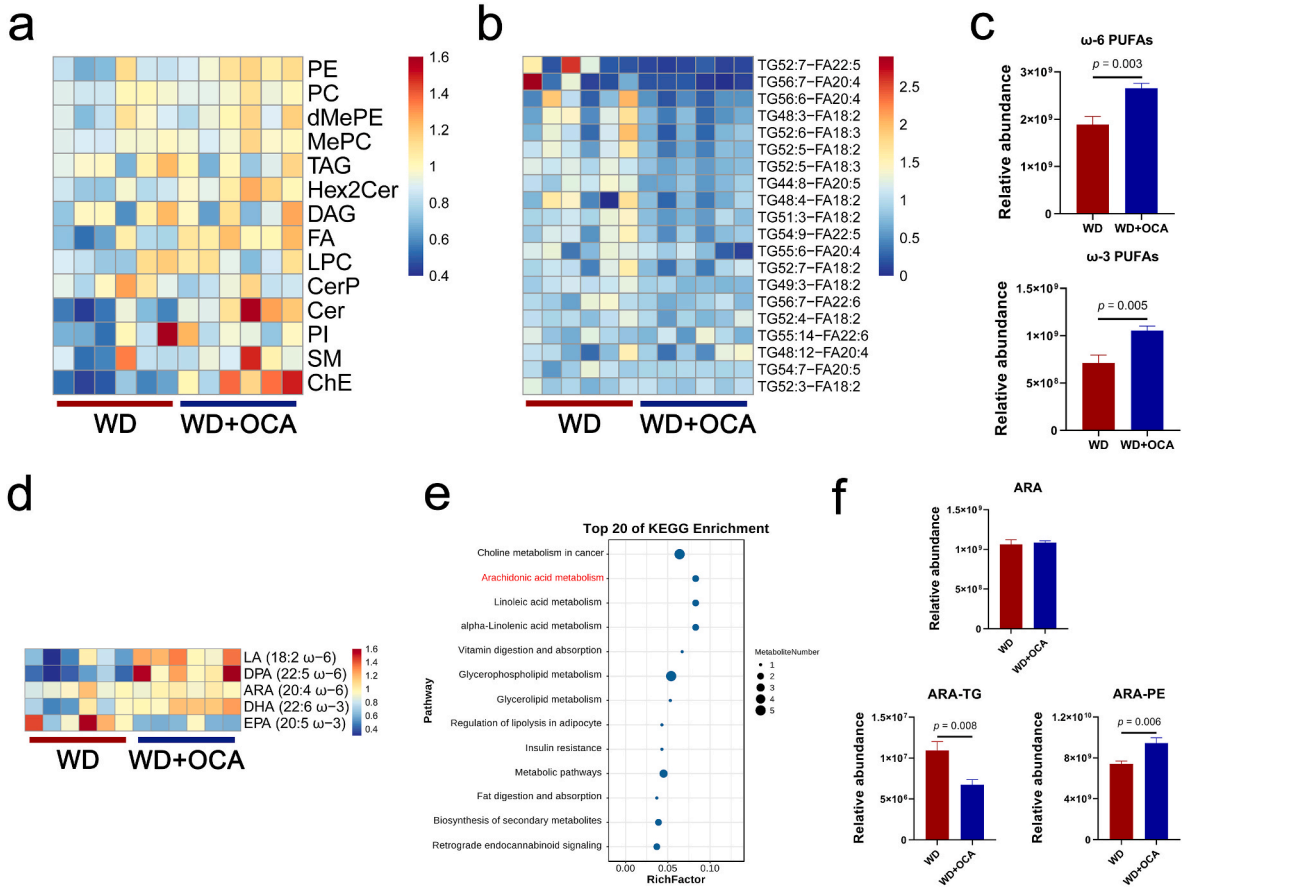

Fig. 6. OCA selectively alters hepatic lipid profiles. (a) Heatmap of hepatic lipid classes. (b) Lipidomic analyses of triglycerides (TG) species containing fatty acid with two or more double bonds (PUFA). (c) Free ω-3 and ω-6 PUFAs quantification. (d) Classes of ω-3 and ω-6 PUFAs. (e) KEGG enrichment analysis between WD-fed and OCA-treated mice. (f) Hepatic concentrations of ARA, ARA-containing TG and ARA-containing PE. n = 6 per group. Data are presented as mean ± SEM. LA, linoleic acid. DPA, docosa-pentaenoic acid. ARA, arachidonic acid. DHA, doco-sahexaenoic acid. EPA, eicosapentaenoic acid. TG, triglycerides. PE, phosphatidylethanolamine.

containing ARA (ARA-PIs and ARA-PCs) remained unchanged (Fig. S5). Moreover, OCA elevated hepatic concentration of C16:0 ceramides, which mediate most of lipotoxic effects of ceramides (Figs. S6a and b) [43]. Based on the lipidomic results, we could conclude that OCA elevated levels of free ω-6 PUFAs and ARA-PEs, which are susceptible to lipid peroxidation and subsequently result in lipitoxicity.

2.6. Lipid peroxide-mediated ferroptosis accounted for HSC activation

ω-3 PUFAs and ω-6 PUFAs are precursors for lipid peroxides and have been reported to result in ferroptosis [44–46], thus we assumed that ARA-PEs enriched by OCA were peroxided, further inducing ferroptosis and lipitoxicity. To verify whether hepatic ferroptosis exists in NASH, TUNEL staining was conducted, suggesting OCA treatment could not alleviate WD-induced hepatocellular death (Figs. S7a and b). Further, hepatic iron concentration indicated OCA slightly aggravated Fe^{2+} overload in NASH (Fig. 7a). Consistently, hepatic mRNA levels of *anti*-ferroptosis genes *SLC7A11* and *GPX4* were down-regulated (Fig. 7b), while their ileum mRNA levels were not significantly regulated (Fig. S7c). Anti-apoptosis genes also exhibited no difference among groups, demonstrating that apoptosis seldomly participated in NASH progression in this model (Fig. S7d).

To further identify key lipid peroxide participating in hepatic ferroptosis and fibrosis, we employed targeted oxylipin omics using UPLC-ESI-MS. Results exhibited that WD-induced elevations in serum levels of ARA and its pro-inflammatory products PGE2 and LXA4 were reversed by OCA (Fig. S8a). DHA-derived, EPA-derived and ARA-derived oxylipins were concentrated in circulation after OCA treatment, among which 8,9-diHETE, 17,18-EpETE and 12-HHTrE (12-HHT) were the most enriched (Fig. 7c and d). Spearman's analysis indicated gut microbes *Bacteroides* and *Helicobacter* were positively related with 12-HHT (Fig. S9). Additionally, OCA significantly up-regulated expressions of ARA-metabolizing enzymes (notably COX2 and LOX5, responsible for generating 12-HHT and HETEs, respectively) (Fig. S8b), suggesting that gut microbiota-derived signals may interact with liver lipid peroxidation to generate oxylipin 12-HHT and induce ferroptosis.

To verify the toxic impact of ARA-derived 12-HHT on hepatocytes and HSCs, we incubated human hepatocyte cell lines L-02 and human HSC cell lines LX-2 with 12-HHT for further cell viability and ferroptotic gene expression experiments. Surprisingly, an evident decrease in cell viability was detected when 12-HHT concentration was increased to 1 μM, which also exhibited dose-dependent inhibitory effect, while LX-2 exhibited no significant difference (Fig. S10a). In line with the cell vitality assay, mRNA levels of *SLC7A11* and *GPX4* were higher in LX-2 (Fig. 7e), suggesting hepatocytes were more sensitive to 12-HHT-induced ferroptosis than HSCs. Further, 12-HHT-induced elevations in MDA levels, lipid peroxidation and ferroptotic gene expressions as well as reductions in cell viability were similar to the phenotype induced by erastin, a ferroptosis inducer, which could be reversed by ferroptosis inhibitor Fer-1 and NAC (Fig. 7f and g, Figs. S10b and c). Interestingly, we adopted a lipid peroxidation inhibitor PTX, which exhibited considerable effects in decreasing MDA levels and regulating ferroptotic gene expressions comparable with Fer-1 or NAC (Fig. 7f and g, Fig. S10c).

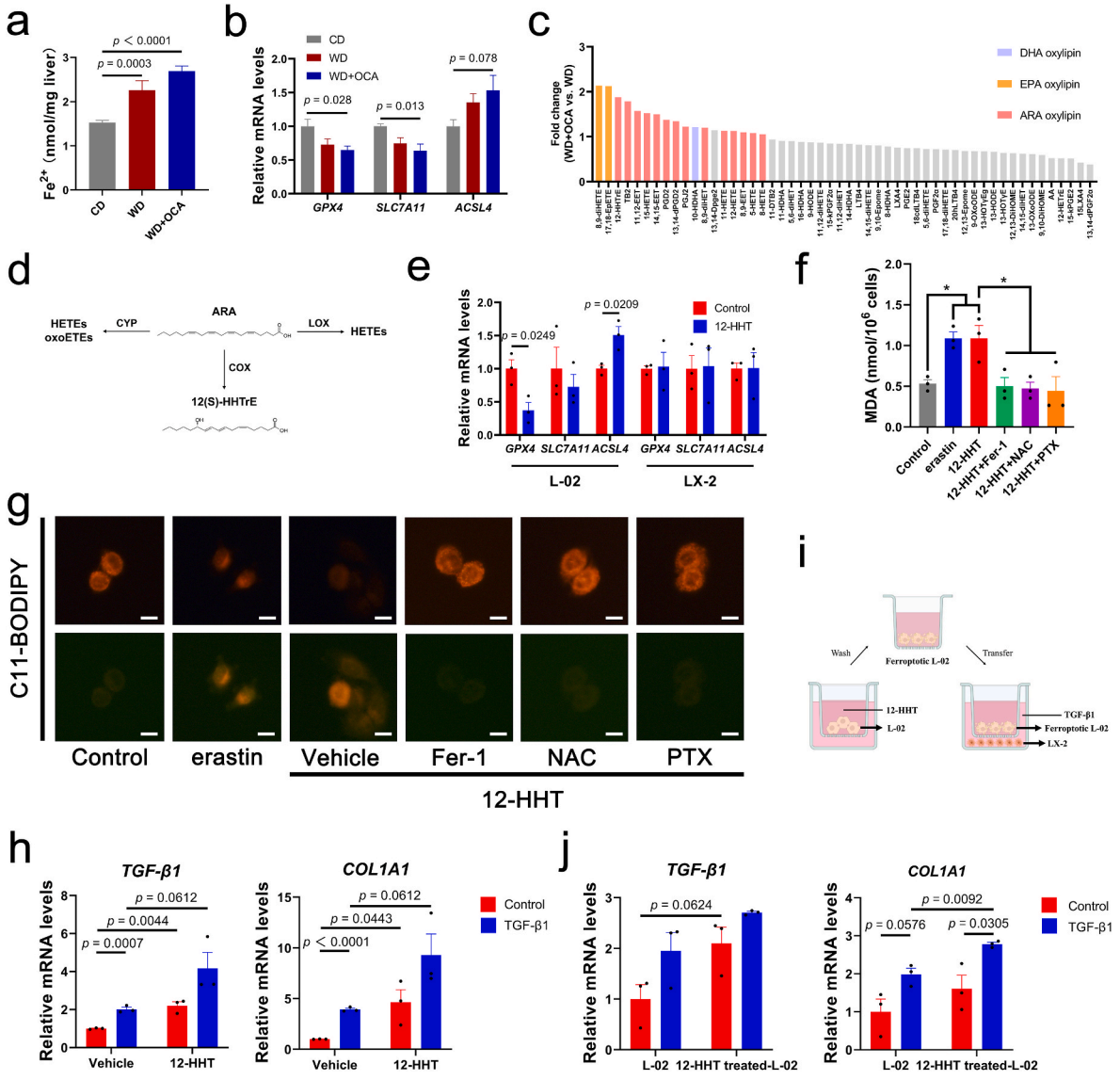

Fig. 7. PUFA-derived lipid peroxide 12-HHTrE induces hepatocyte ferroptosis and activates HSCs. (a) Hepatic Fe^{2+} quantification (n = 8 per group). (b) Relative mRNA expressions of ferroptosis genes (n = 8 per group) (c) Fold change of differential lipid peroxides between OCA-treated and WD-fed mice based on targeted peroxide omics (n = 6 per group). (d) Metabolic diagram of ARA-derived oxylipins. (e) Expressions of ferroptosis genes of 12-HHT-treated L-02 or LX-2 cells (n = 3 per group). (f) MDA levels of L-02 treated with erastin or 12-HHT with or without ferroptosis inhibitor Fer-1, NAC and PTX (n = 3 per group). (g) Lipid peroxidation of L-02 with different treatments detected by C11-BODIPY, scale bar 10 μm. (h) Expressions of fibrotic genes of LX-2 treated with 12-HHT (n = 3 per group). (i) Co-cultrue model using transwell assay. (j) Expressions of fibrotic genes of LX-2 co-cultured with 12-HHT-treated L-02 (n = 3 per group). Data are presented as mean ± SEM. *$p < 0.05$. 12-HHTrE, 12S-hydroxy-5Z,8E,10E-heptadecatrienoicacid. Fer-1, ferrostatin-1. NAC, N-Acetyl-L-cysteine. PTX, Pentoxifylline.

We further investigated whether 12-HHT directly activates HSCs, and elevated expressions of fibrotic genes were detected regardless of TGF-β1 presence (Fig. 7h). To provide a crosstalk between ferroptotic hepatocytes and activated HSCs, we asked whether ferroptotic L-02, which is a typical event witnessed in the process of liver fibrosis, may represent the key triggers in activating HSCs. The effect of hepatocyte ferroptosis on HSC activation was further assessed in a co-culture model (Fig. 7i). As expected, LX-2 incubated with ferroptotic L-02 exhibited elevated expressions of fibrotic genes *TGF-β1* and *COL1A1* (Fig. 7j).

To conclude, these results indicated that ω-6 PUFA ARA-derived 12-HHT activated HSCs either directly or indirectly by inducing hepatocyte ferroptosis.

2.7. Combined OCA and lipid peroxidation inhibitor PTX ameliorated NASH-related ferroptosis and advanced fibrosis

Considering ferroptosis is a key pathological stimulus in the development of NASH-related liver fibrosis and the impact of OCA against hepatocellular ferroptosis is limited, it is reasonable to predict that OCA combined with lipid peroxidation inhibitor may exhibit additively anti-fibrotic effect. Thus, we further assessed synergistic anti-fibrotic effect of OCA and PTX on WD-fed mice (Fig. 8a). ARA-derived oxylipins, predominantly 12-HHT, was significantly reduced after PTX supplement (Fig. 8b, Fig. S11). Notably, supplement of PTX ameliorated hepatic ROS overload (Fig. 8c) and regulated hepatic expressions of oxidative genes and ferroptotic genes (Fig. 8d), which were in line with elevated GSH and reduced MDA levels (Fig. 8e). Importantly, combination of OCA and PTX considerably reduced deposition of collagen fiber and α-SMA expression as well as down-regulating expressions of fibrotic genes

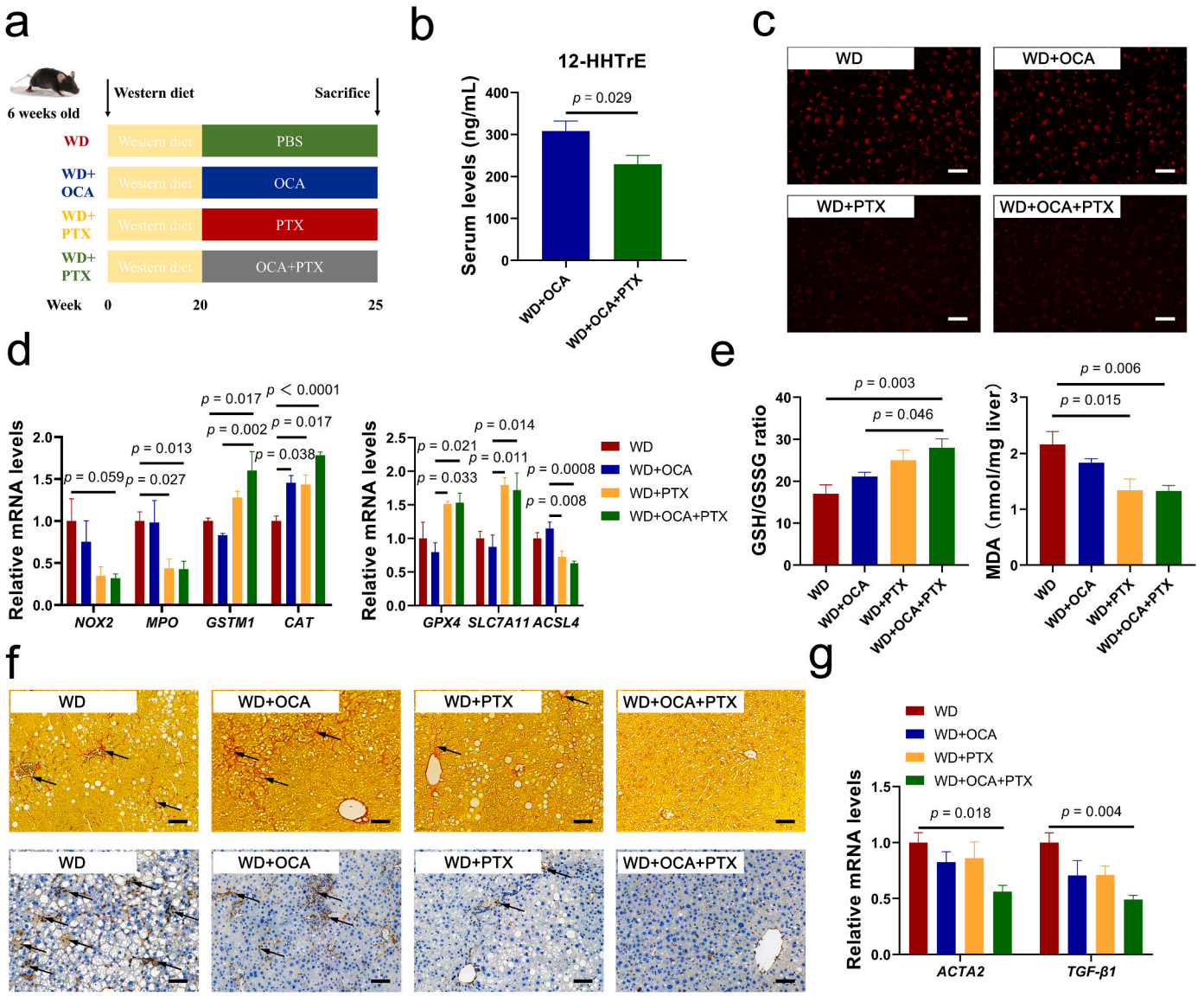

Fig. 8. Combined OCA and lipid peroxidation inhibitor PTX impede ferroptosis and advanced fibrosis in NASH. (a) Experimental design. (b) Serum levels of 12-HHT (n = 6–7 per group). (c) Representative images of liver sections with dihydroethidium (DHE) staining, scale bar 40 μm. (d) Liver mRNA expressions of oxidative-damage-related genes *NOX2*, *MPO*, *GSTM1*, *CAT* and ferroptosis-related genes *GPX4*, *SLC7A11* (n = 5–6 per group). (e) Hepatic concentrations of oxidative stress biomarkers GSH and MDA (n = 5–8 per group). (f) Representative images of liver sections with Sirius Red and α-SMA immunohistochemistry staining, scale bar 80 μm. (g) Liver mRNA expressions of fibrosis biomarkers *ACTA2* and *TGF-β1* (n = 5–6 per group). Data are presented as mean ± SEM. 12-HHTrE, 12S-hydroxy-5Z,8E,10E-heptadecatrienoicacid. (For interpretation of the references to color in this figure legend, the reader is referred to the Web version of this article.)

(Fig. 8f and g).

Nevertheless, combination of OCA and PTX exhibited no further alleviation on liver function and hyperlipidemia compared to OCA treatment (Fig. S12a). In addition, PTX evidently improved glucose dysfunction, while the combination abolished this metabolic benefit of PTX (Figs. S12b and c). This may be explained by elevations in insulin-resistance-related lipid Cer due to OCA (Fig. S12d).

3. Discussion

FXR agonist OCA is a novel treatment for NAFLD, which has exhibited beneficial effects in hepatic lipogenesis, steatosis and gluconeogenesis by modulating BA metabolism [5,47], whereas specific mechanisms on how OCA improves NASH have not been systematically elucidated. Additionally, liver fibrosis of NASH patients was only slightly reduced upon OCA treatment in recent phase III clinical trial [9]. Therefore, it's essential to identify which driver in NASH progression impairs the anti-fibrotic effect of OCA, and the underlying mechanism may be significant in determining the efficiency of OCA in clinical practice.

Overloaded oxidative stress and impaired antioxidant defense have been documented to induce hepatocyte death and promote progressive NASH fibrosis [31,48]. We indicated that OCA cannot evidently ameliorate imbalance between pro-oxidative and anti-oxidative systems in the liver, ileum and serum, suggesting its limited anti-oxidative effect. However, these findings are not consistent with former studies showing that OCA could prevent mitochondrial dysfunction and oxidative stress by activating liver FXR pathway [49,50]. Considering that OCA obviously activates liver *FXR-SHP* axis, we postulate that there may exist other mechanisms weakening the FXR-mediated anti-oxidative effect of OCA.

BA, especially secondary BA could perturbate cell membrane owning to their fat-soluble capacity, which causes the release of ARA from the membrane and ultimately contributes to accumulated ROS in the

hepatocyte [51]. We demonstrated that OCA evidently inhibits classical pathway of BA synthesis rather than alternative pathway, characterized by depleted CA and elevated CDCA. CDCA has been recognized as a toxic BA which will bind to mitochondria, causing mitochondrial dysfunction and ROS accumulation [51–53]. Similarly, we found CDCA dose-dependently induced mitochondrial ROS overload and lipid peroxidation in the hepatocytes. Additionally, tauro-conjugated BAs were declined either in the serum or stool in response to the OCA treatment. Since microbiota-derived BSH mediated deconjugation of conjugated BAs in the enterohepatic circulation of bile acids [51], these results indicate that the gut microbiota may be associated in CDCA production and the pro-oxidative effect of OCA.

Intestine is the primary target of OCA absorption where gut microbes colonize, and the gut microbiota is recognized to participate in NAFLD progression through mediating fat storage and redox signals [40,54]. Our results demonstrated that OCA reshaped community composition, especially enriching *Bacteroides* and *Helicobacter*. *Bacteroides* is a major BSH bacteria which could deconjugate TCDCA to generate CDCA [55], and *Helicobacter* is recognized as a key microbial stimulus of gut ROS production through interaction with intestinal epithelial cells [56]. To support, these two microbes were positively correlated with liver and ileum ROS levels, respectively. And intestinal decontamination with ABX abolished microbiota-mediated oxidative stress and rescued anti-oxidative effect of OCA. These data may partly explain another mechanism on OCA influencing liver oxidative stress via gut microbiota-liver axis independent of FXR activation.

In our study, WD-induced MDA accumulation was not improved by OCA, suggesting that hepatic lipitoxicity of lipid peroxides under oxidative stress may be a key mediator deteriorating liver fibrosis. Lipotoxicity in NASH is primarily caused by increasing hepatic levels of saturated fatty acids (SFAs), free cholesterol (FC), glycerophospholipids, sphingolipids and ω-3 PUFAs, or PUFA-derived specialized proresolving mediators [57,58]. Coincidentally, OCA has been reported to primarily reduce hepatic concentration of TG containing PUFAs [42]. Our lipidomic data suggested that OCA selectively modulated hepatic lipid profiles, particularly lowering TG containing PUFAs whereas elevating free PUFAs in the liver. Free ω-6 PUFAs (LA, DPA and ARA) were concentrated after OCA treatment, which provides materials for lipid peroxidation induced by oxidative stress. Oxylipin omics additionally indicated that oxylipins, primarily ω-6 PUFA ARA-derived HHTs, EETs and HETEs, were produced in response to microbial signals in this process.

Generally, vast majority of ARAs exist in the form of glycerophospholipids including PC, PE and PI, and these anchored ARAs could be peroxided under oxidative stimuli, further impairing cell membrane and leading to ferroptosis [59,60]. Notably, we found ARA-PEs were enriched by OCA treatment. TG is a major lipid class forming lipid droplet in NAFLD, and they could protect against lipitoxicity due to lipid overload by combining the toxic fatty acids (FAs) [45,57]. Moreover, FAs storage in LDs could be mobilized and oxidized to fulfill cellular needs [61]. Therefore, we hypothesize that OCA lipolyzed ARA-TGs to release ARAs, which were further incorporated to glycerophospholipids for utilization. ARA-PEs or its elongation product, adrenic acid (C22:4), are regarded as key phospholipids that undergo oxidation and drive cells towards ferroptosis [62]. Previous studies have demonstrated the reduction of ARAs in FFA, TG and PC and elevation of ARA-derived lipoxygenase (LOX) oxylipins 5-HETE, 8-HETE, 11-HETE and 15-HETE during NASH progression [63,64]. Moreover, acute-on-chronic liver failure patients harbors higher plasma levels of free ARA but not other PUFAs [65], which indicates the vital role of ARA and associated oxylipins in liver lipidoxicity.

In this study, we identified up-regulation of ARA-metabolizing enzymes and enrichments of ARA-derived oxylipins HETEs and 12-HHT mediated by OCA. Since HETEs have been widely studied to induce cellular membrane rupture and ferroptosis [66,67], we further investigated the potential lipidoxicity of microbiota-related 12-HHT and identify ferroptosis as the primary type of hepatic cell death mediated by 12-HHT. The role of ferroptosis is contradictory, as hepatocyte ferroptosis is a manifestation of liver fibrosis whereas targeting HSC ferroptosis is an emerging therapy for inhibiting HSC activation [68]. We found HSCs showed stronger resistance to 12-HHT-mediated ferroptosis than hepatocytes at the pathological concentration of 12-HHT (1 μM). Further, 12-HHT could upregulate profibrotic expressions of HSCs in two ways: directly or trigger hepatocyte ferroptosis to activate HSCs. These evidence indicated that lipid peroxidation may serve as a key driver of NASH-related fibrosis which reverses the anti-fibrotic effect of OCA.

Till now, there is no effective treatment for NASH due to its complicated profiles implicating lipid metabolism, BA homeostasis, oxidative stress, insulin resistance, lipotoxicity, etc. [69]. Thus, combined therapy targeting multiple aspects is necessary for the treatment of NASH. Considering that OCA could induce lipid peroxidation-mediated ferroptosis, we assume that inhibition of lipid peroxidation could be a potential therapeutic strategy for NASH-related fibrosis. The feasibility of this strategy was subsequently illustrated by PTX, a lipid peroxidation inhibitor proved to reduce plasma levels of ω-6 PUFAs-derived oxidized lipids HETEs, HODEs and oxoODEs [70]. Consistently, our data indicated that PTX significantly decreased lipid peroxidation and subsequent ferroptosis similar to ferroptosis inhibitor Fer-1 or NAC. Meanwhile, PTX could rescue the unsatisfactory effect of OCA on lipid peroxidation and ferroptosis, and PTX supplement additively alleviates OCA-unresponsive liver fibrosis.

Additionally, we found PTX ameliorates insulin resistance, which could be offset by OCA when combined used, indicating its contradictory effect on glucose homeostasis. One possible explanation is that accumulated ceramides in the liver, which is associated with activation of gut FXR pathway by OCA [71], accounts for poor insulin resistance [72,73]. Lipid peroxidation inhibitor PTX undermining ferroptosis could not rescue poor effect of OCA to restore insulin resistance, demonstrating this may be related with Cer elevations rather than ferroptosis.

A major limitation in this study is that we demonstrated the critical role of the gut microbiota mediated by OCA in hepatic lipid peroxidation and identify related microbes, yet specific mechanisms on how OCA mediates shifts in microbial composition remains unclear. Considering BAs and short chain fatty acids (SCFA) are key determinants in maintaining the dynamic communication between the host and microbiota [74,75], mechanisms on how OCA-mediated BA and SCFA spectrum reshapes microbiota worth further elucidation. Germ-free mice could be considered to mine underlying mechanism and verify the effect of specific microbes on lipid peroxidation at species level. Our lipidomic data showed reductions in ARA-TGs and elevations in free ARAs and ARA-PEs, thus we assume that ARAs may be released from TG to incorporate into PE to be further oxidized, this hypothesis should be further verified with ARA isotope-tracing analysis in the subsequent study. Since we note that OCA induces ARA-derived ferroptosis with alternations in BA spectrum, gut microbiome and hepatic lipid spectrum, we clarify that humans and mice have different BA pools, gut microbial compositions and hepatic lipid profiles. Similarly, humans and mice share distinctive mass-specific metabolic rate, and this results in different pools of ROS, a by-product of energy metabolism in the mitochondria, and different capacity to maintain cellular homeostasis, which finally contributes to different susceptibility to ROS-induced cell death [76]. Therefore, there may have additional mechanism in humans compared to mice experiment, indicating further random clinical trial should be processed to prove the synergy of this combination on NASH-fibrosis patients.

In summary, the pro-fibrotic effect of ARA-derived oxylipin 12-HHT underpins a critical contribution of lipid peroxidation and ferroptosis to liver fibrosis in NASH. Our results demonstrate the unsatisfactory anti-fibrotic effect of OCA on NASH-fibrosis may be due to ferroptosis induced by its mediated oxylipin spectrum. Crosstalk among BA metabolism, gut microbiota and lipid metabolism identifies a vital role of gut

microbiota on OCA-mediated ferroptosis. Importantly, we found OCA synergized with lipid peroxidation inhibitor PTX additively alleviate OCA-unresponsive fibrosis (Fig. 9).

4. Method

4.1. Drug preparation

OCA (Sunshine Chemical, Wuhan, China) was freshly suspended in 0.5% methyl cellulose (MC) in a dosing volume of 6 g/L and ultrasonicated prior to use. Pentoxiphylline (PTX, Alarddin, Shanghai, China) was dissolved in normal saline solution at a dose of 10 g/L and filtered through a 0.22 μm filter before use.

4.2. Animal administration

Male specific pathogen free (SPF) C57BL/6J mice were kept at room temperature with a controlled 12-12 h light-dark cycle. All mice were administrated after an one-week acclimatization.

To investigate the impact of OCA on NASH-related fibrosis, mice were treated with (a) control diet with vehicle (CD group); (b) western diet (high fat diet plus high fructose/glucose in drinking water) with vehicle (WD group); (c) western diet with OCA (30 mg/kg). OCA were administrated by oral gavage daily from the 20th week for 5 weeks.

To investigate the role of microbiota in OCA-mediated lipid peroxidation, WD-fed mice were pretreated with a 7-day antibiotics cocktail to remove gut microbes, including vancomycin (100 mg/kg), neomycin sulfate (200 mg/kg), metronidazole (200 mg/kg) and ampicillin (200 mg/kg). Then mice were treated with OCA (30 mg/kg) for 7 days.

To investigate the synergetic effect of OCA and lipid peroxidation inhibitor on oxidative-stress-associated fibrosis in NASH, mice were treated with (a) western diet with vehicle; (b) western diet with OCA (30 mg/kg); (c) western diet with PTX (100 mg/kg); (d) western diet with OCA (30 mg/kg) and PTX (100 mg/kg). PTX was intervened by intraperitoneal injection daily. OCA and PTX were administrated from the 20th week for 5 weeks.

4.3. Cell culture

The human hepatocyte cell line L-02 and HSC cell line LX-2 were purchased from ATCC (Manassas, VA, USA). Both cells were cultured with Dulbecco's modified Eagle's medium (DMEM, Gibco, MD, USA) supplemented with 10% fetal bovine serum (FBS, Gibco) and 1% penicillin/streptomycin (Beyotime, Shanghai, China) in a 37 °C incubator with 5% CO_2.

To investigate whether CDCA induces liver ROS accumulation, L-02 cells were treated with 0, 20, 50, 100, 200 μM CDCA for 24 h, and harvested for lipid peroxidation assays.

To investigate whether 12-HHT induces ferroptosis in hepatocytes and HSCs and directly activates HSCs, LX-2 and L-02 cells were cultured with 1 μM 12-HHT for 24h, respectively, and harvested for further assays.

To investigate whether 12-HHT-induced hepatocellular death could be reversed by ferroptosis inhibitor, L-02 cells were cultured with erastin (5 μM) or 12-HHT (1 μM) in the presence or absence of Fer-1 (1 μM), NAC (2 mM) or PTX (1 mM) for 24 h, and harvested for further assays.

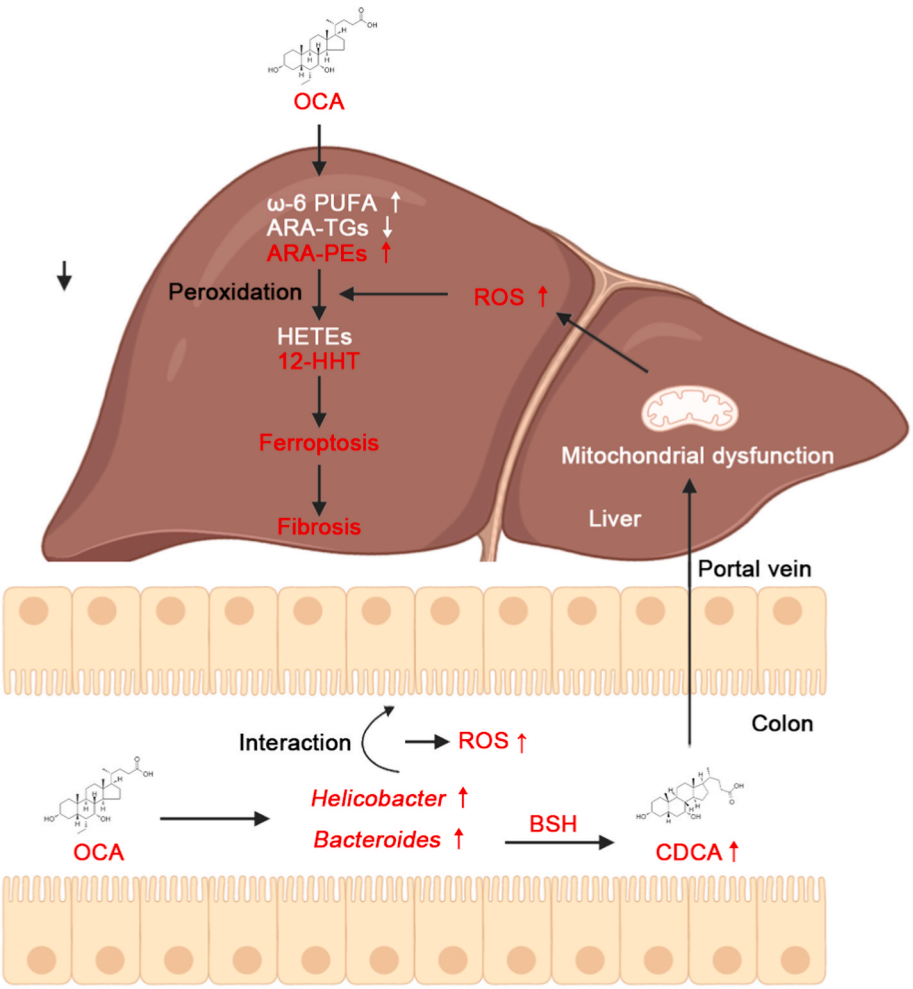

Fig. 9. Proposed mechanism for poor anti-fibrotic effect of OCA against NASH. OCA alters gut microbial composition, notably enriching oxidative stress-corresponding *Helicobacter* and *Bacteroides*. *Helicobacter* is related with gut ROS accumulation, and *Bacteroides* induces liver ROS overload through BSH-mediated excessive CDCA generation from deconjugation of conjugated bile acids. Additionally, OCA selectively regulates hepatic lipid profiles, characterized as reductions in ARA-TGs and elevations in ω-6 PUFAs and ARA-PEs, which are susceptible to lipid peroxidation. 12-HHT is identified as a key effector impairing *anti*-ferroptotic and anti-fibrotic effect of OCA.

4.4. Transwell assay

To investigate whether 12-HHT promotes HSC activation by ferroptotic hepatocytes, a modified co-culture model was enrolled using transwell chambers with 8-μm pores. Briefly, LX-2 cells were plated in a 6-well plate, while L-02 cells were plated on the upper permeable chamber in another 6-well plate. L-02 cells were incubated with 1 μM 12-HHT or vehicle for 24 h. Then the cell-culture inserts were washed with PBS, replaced with new medium and transferred onto the plate containing LX-2 cells. After co-culture for 24 h, LX-2 cells were harvested for further assays.

4.5. Serum biochemistry

Seral levels of alanine aminotransferase (ALT), aspartate aminotransferase (AST), total cholesterol (TC), triglyceride (TG) and total bile acid (TBA) were quantified through the automatic blood biochemical analyzer (SRL., Tokyo, Japan).

4.6. Serum cytokine and chemokine assay

Seral concentrations of cytokines and chemokines including IL-1β, IL-3, IL-5, IL-6 and IL-10 were quantified through a Bio-plex Mouse Cytokine kit (Bio-Rad, CA, USA) according to the manufacturer's instructions.

4.7. Liver ELISA assays

Hepatic concentrations of TC, TG, superoxide dismutase (SOD) and glutathione (GSH) were quantified by commercial ELISA kits (Abcam, MA, USA; Sigma-Aldrich Corp, MO, USA). Briefly, liver sections were homogenized and centrifuged to harvest supernatant for further measurement.

4.8. Serum ELISA assays

Seral levels of free fatty acid (FFA), glucagon-like peptide-1 (GLP-1), peptide YY (PYY), GSH and SOD activity were assessed by commercial ELISA kits (Abcam; RayBiotech, GA, USA).

4.9. Lipid peroxidation assays

The lipid peroxidation level was evaluated by malondialdehyde (MDA) quantification, C11-BOPIY and Mito-Tracker Red CMXRos staining.

Briefly, MDA quantification was conducted using a commercial ELISA kit by homogenizing 10 mg of liver sections or 10^6 cells. To assess intracellular ROS, cells were harvested and incubated with 2 μM C11-BODIPY or 200 nM Mito-Tracker Red CMXRos at 37 °C for 30 min. Then, images were obtained by an LSM T-PMT confocal microscope (Zeiss).

4.10. Intraperitoneal glucose tolerance test (IGTT)

IGTT was conducted one week before sacrifice as previously described [77]. Briefly, mice were fasted for 16 h and then injected with 2 g/kg glucose intraperitoneally. Blood glucose levels were assessed at 0. 15, 30, 60, 90, 120 min after injection with a glucometer (Roche, Basel, Switzerland).

4.11. Histopathology analysis

Fresh liver sections were fixed in 10% paraformaldehyde for 24 h, embedded in paraffin and cut into 2 μm-thickness slices. Slices were then stained with hematoxylin and eosin (H&E) and Sirius Red. We applied a NAFLD activity score (NAS) system to estimate the degree of NAFLD progression as previously described [78]. Fibrosis index was evaluated based on Sirius Red staining according to NAS.

Frozen liver sections in 4 μm-thickness were fixed in 4% neutralized formaldehyde and stained with Oil Red-O, and the area of lipid droplet was calculated to assess hepatic lipid accumulation by ImageJ.

Hepatocyte death was detected by a terminal deoxynucleotidyl transferase dUTP nick end labeling (TUNEL) assay (Vazyme, Nanjing, China) according to the protocol. The percentage of positive cells was counted using Image J.

4.12. Dihydroethidium (DHE) staining and reactive oxygen species (ROS) quantification

Frozen liver and ileum sections were stained with DHE to assess ROS concentrations.

A ROS ELISA kit was employed to quantify ROS levels in the liver and ileum (Biolab, Beijing, China).

4.13. Immunohistochemistry staining

Paraffin-embedded liver sections were successively incubated with α-SMA and MPO antibodies (Abcam) and HRP-conjugated secondary antibodies (Beyotime). The positive area of α-SMA was measured using ImageJ IHC profiler to evaluate fibrosis progression.

4.14. Cell viability assay

An enhanced Cell Counting Kit-8 (CCK-8; Beyotime) was used to measure cell viabilities. L-02 and LX-2 cells were seeded in 96-well plates at a density of 5000 per well and cultured with 0–5 μM 12-HHT for 24h. Cells were incubated with CCK8 assay for 2 h, and the absorbance were measured at 450 nm. For each condition, 6 independent biological duplicates were assessed.

4.15. BSH activity assay

Bacterial BSH activity was measured via quantifying the liberated taurine released from tauro-conjugated bile salts based on the previous study with several modifications [79,80]. Briefly, 50 mg of stool was homogenized, lysed on ice and centrifuged to extract fecal total proteins. Then the protein extract was quantified by a BCA assay and diluted to 1 mg/ml in 3 mM sodium acetate. BSH reaction was carried out by adding 170 μL of 3 mM sodium acetate and 20 μL of 1 mM TDCA or TUDCA to 10 μL of protein extract under incubation at 37 °C for 30 min. Then reactions were stopped by plunging the samples into dry ice. For the second reaction, thawed mixture was centrifuged and 20 μL of supernatant was mixed with 80 μL of distilled water and 1.9 mL of ninhydrin reagent (0.5 mL of 1% (wt/vol) ninhydrin in 0.5 M sodium citrate buffer, pH 5.5; 1.2 ml of 30% (wt/wt) glycerol; and 0.2 ml of 0.5 M sodium citrate buffer, pH 5.5), mixed thoroughly and boiled for 15 min. After subsequent cooling, the absorbance at 570 nm was determined using taurine as standard. BSH activity was measured based on the generation of CDCA from TCDCA.

4.16. Iron assessment

Iron quantification was conducted using a commercial iron assay kit (Abcam) according to the instructions. Briefly, fresh liver tissue was washed with PBS, homogenized and measured using a colorimetric microplate reader.

4.17. RNA extraction and real-time quantitative PCR

Total RNA of liver or cells were extracted by a RNeasy Mini Kit (Qiagen, CA, USA) following manufacturer's protocols and assessed by VIIA7 real-time PCR system (Applied Biosystems, CA, USA). Relative

mRNA expressions were normalized to the levels of the gene *GAPDH*. The primer sequences are listed in Supplementary Table 1.

4.18. Statistical analysis

Kolmogorov-Smirnov test was employed to evaluate the normality of the data. One-way ANOVA was used to check differences among more than two groups with normal distributions, and Turkey's test was performed to adjust for multiple comparisons; otherwise, the Kruskal-Wallis test was used. Statistical significances in pairwise comparisons were analyzed using Student's *t*-test with normal distribution; otherwise, a Mann-Whitney *U* test was used. ANOSIM was used to test for clustering of microbial communities. Correlations between two parameters were checked by Spearman's rank correlation. IBM SPSS Statistics 20 (SPSS Inc., Chicago, IL, USA), GraphPad Prism 6 (GraphPad Software Inc., IL, USA) and R software were used to analyze data and draw figures. Data are shown as mean ± SEM, and a p value < 0.05 was recognized as statistically significant.

Ethics statement

All procedures were performed in strict accordance with the 2011 National Institutes of Health Guide for the Care and Use of Laboratory Animals and were committed by the Animal Ethics Care Committee of the First Affiliated Hospital, School of Medicine, Zhejiang University.

Declaration of competing interest

The authors declare no conflicts of interest.

Data availability

Data will be made available on request.

Acknowledgement

This study was supported by the National Natural Science Foundation of China (81790631), the National Key Research and Development Program of China (2018YFC2000500, 2021YFA1301104 and 2021YFC2301804), CAMS Innovation Fund for Medical Sciences (2019-I2M-5–045) and Research Project of Jinan Microecological Biomedicine Shandong Laboratory (JNL-2022001A).

Appendix A. Supplementary data

Supplementary data to this article can be found online at https://doi.org/10.1016/j.redox.2022.102582.

References

[1] C.J. Sinal, M. Tohkin, M. Miyata, J.M. Ward, G. Lambert, F.J. Gonzalez, Targeted disruption of the nuclear receptor FXR/BAR impairs bile acid and lipid homeostasis, Cell 102 (2000) 731–744.
[2] W. Huang, K. Ma, J. Zhang, M. Qatanani, J. Cuvillier, J. Liu, B. Dong, X. Huang, D. D. Moore, Nuclear receptor-dependent bile acid signaling is required for normal liver regeneration, Science 312 (2006) 233–236.
[3] K. Ma, P.K. Saha, L. Chan, D.D. Moore, Farnesoid X receptor is essential for normal glucose homeostasis, J. Clin. Invest. 116 (2006) 1102–1109.
[4] Y. Zhang, L.W. Castellani, C.J. Sinal, F.J. Gonzalez, P.A. Edwards, Peroxisome proliferator-activated receptor-gamma coactivator 1alpha (PGC-1alpha) regulates triglyceride metabolism by activation of the nuclear receptor FXR, Genes Dev. 18 (2004) 157–169.
[5] L. Sun, J. Cai, F.J. Gonzalez, The role of farnesoid X receptor in metabolic diseases, and gastrointestinal and liver cancer, Nat. Rev. Gastroenterol. Hepatol. 18 (2021) 335–347.
[6] A. Lleo, G.Q. Wang, M.E. Gershwin, G.M. Hirschfield, Primary biliary cholangitis, Lancet 396 (2020) 1915–1926.
[7] M.F. Abdelmalek, Nonalcoholic fatty liver disease: another leap forward, Nat. Rev. Gastroenterol. Hepatol. 18 (2021) 85–86.
[8] K.V. Kowdley, R. Vuppalanchi, C. Levy, A. Floreani, P. Andreone, N.F. LaRusso, R. Shrestha, J. Trotter, D. Goldberg, S. Rushbrook, G.M. Hirschfield, T. Schiano, Y. Jin, R. Pencek, L. MacConell, D. Shapiro, C.L. Bowlus, A randomized, placebo-controlled, phase II study of obeticholic acid for primary sclerosing cholangitis, J. Hepatol. 73 (2020) 94–101.
[9] Z.M. Younossi, V. Ratziu, R. Loomba, M. Rinella, Q.M. Anstee, Z. Goodman, P. Bedossa, A. Geier, S. Beckebaum, P.N. Newsome, D. Sheridan, M.Y. Sheikh, J. Trotter, W. Knapple, E. Lawitz, M.F. Abdelmalek, K.V. Kowdley, A.J. Montano-Loza, J. Boursier, P. Mathurin, E. Bugianesi, G. Mazzella, A. Olveira, H. Cortez-Pinto, I. Graupera, D. Orr, L.L. Gluud, J.F. Dufour, D. Shapiro, J. Campagna, L. Zaru, L. MacConell, R. Shringarpure, S. Harrison, A.J. Sanyal, Obeticholic acid for the treatment of non-alcoholic steatohepatitis: interim analysis from a multicentre, randomised, placebo-controlled phase 3 trial, Lancet 394 (2019) 2184–2196.
[10] M. Eslam, R. Alvani, G. Shiha, Obeticholic acid: towards first approval for NASH, Lancet 394 (2019) 2131–2133.
[11] F. Nevens, P. Andreone, G. Mazzella, S.I. Strasser, C. Bowlus, P. Invernizzi, J. P. Drenth, P.J. Pockros, J. Regula, U. Beuers, M. Trauner, D.E. Jones, A. Floreani, S. Hohenester, V. Luketic, M. Shiffman, K.J. van Erpecum, V. Vargas, C. Vincent, G. M. Hirschfield, H. Shah, B. Hansen, K.D. Lindor, H.U. Marschall, K.V. Kowdley, R. Hooshmand-Rad, T. Marmon, S. Sheeron, R. Pencek, L. MacConell, M. Pruzanski, D. Shapiro, A placebo-controlled trial of obeticholic acid in primary biliary cholangitis, N. Engl. J. Med. 375 (2016) 631–643.
[12] R.F. van Golen, P.B. Olthof, D.A. Lionarons, M.J. Reiniers, L.K. Alles, Z. Uz, L. de Haan, B. Ergin, D.R. de Waart, A. Maas, J. Verheij, P.L. Jansen, S.W.O. Damink, F. G. Schaap, T.M. van Gulik, M. Heger, FXR agonist obeticholic acid induces liver growth but exacerbates biliary injury in rats with obstructive cholestasis, Sci. Rep. 8 (2018), 16529.
[13] T. Zhang, S. Feng, J. Li, Z. Wu, Q. Deng, W. Yang, J. Li, G. Pan, Farnesoid X receptor (FXR) agonists induce hepatocellular apoptosis and impair hepatic functions via FXR/SHP pathway, Arch. Toxicol. (2022), https://doi.org/10.1007/s00204-022-03266-6.
[14] J. Zhou, N. Huang, Y. Guo, S. Cui, C. Ge, Q. He, X. Pan, G. Wang, H. Wang, H. Hao, Combined obeticholic acid and apoptosis inhibitor treatment alleviates liver fibrosis, Acta Pharm. Sin. B 9 (2019) 526–536.
[15] G.M. Hirschfield, A. Mason, V. Luketic, K. Lindor, S.C. Gordon, M. Mayo, K. V. Kowdley, C. Vincent, H.C. Bodhenheimer Jr., A. Parés, M. Trauner, H. U. Marschall, L. Adorini, C. Sciacca, T. Beecher-Jones, E. Castelloe, O. Böhm, D. Shapiro, Efficacy of obeticholic acid in patients with primary biliary cirrhosis and inadequate response to ursodeoxycholic acid, Gastroenterology 148 (2015) 751–761, e8.
[16] S. Al-Dury, A. Wahlström, K. Panzitt, A. Thorell, M. Ståhlman, M. Trauner, P. Fickert, F. Bäckhed, L. Fändriks, M. Wagner, H.U. Marschall, Obeticholic acid may increase the risk of gallstone formation in susceptible patients, J. Hepatol. 71 (2019) 986–991.
[17] T. Tsuchida, S.L. Friedman, Mechanisms of hepatic stellate cell activation, Nat. Rev. Gastroenterol. Hepatol. 14 (2017) 397–411.
[18] R. Loomba, S.L. Friedman, G.I. Shulman, Mechanisms and disease consequences of nonalcoholic fatty liver disease, Cell 184 (2021) 2537–2564.
[19] H. Li, P. Ding, B. Peng, Y.Z. Ming, Cross-talk between hepatic stellate cells and T lymphocytes in liver fibrosis, Hepatobiliary Pancreat. Dis. Int. 20 (2021) 207–214.
[20] J. Gautheron, G.J. Gores, C.M.P. Rodrigues, Lytic cell death in metabolic liver disease, J. Hepatol. 73 (2020) 394–408.
[21] F. Lin, W. Chen, J. Zhou, J. Zhu, Q. Yao, B. Feng, X. Feng, X. Shi, Q. Pan, J. Yu, L. Li, H. Cao, Mesenchymal stem cells protect against ferroptosis via exosome-mediated stabilization of SLC7A11 in acute liver injury, Cell Death Dis. 13 (2022) 271.
[22] S. Tsurusaki, Y. Tsuchiya, T. Koumura, M. Nakasone, T. Sakamoto, M. Matsuoka, H. Imai, C. Yuet-Yin Kok, H. Okochi, H. Nakano, A. Miyajima, M. Tanaka, Hepatic ferroptosis plays an important role as the trigger for initiating inflammation in nonalcoholic steatohepatitis, Cell Death Dis. 10 (2019) 449.
[23] L. Yu, M. He, S. Liu, X. Dou, L. Li, N. Gu, B. Li, Z. Liu, G. Wang, J. Fan, Fluorescent egg white-based carbon dots as a high-sensitivity iron chelator for the therapy of nonalcoholic fatty liver disease by iron overload in zebrafish, ACS Appl. Mater. Interfaces 13 (2021) 54677–54689.
[24] J.E. Nelson, L. Wilson, E.M. Brunt, M.M. Yeh, D.E. Kleiner, A. Unalp-Arida, K. V. Kowdley, Relationship between the pattern of hepatic iron deposition and histological severity in nonalcoholic fatty liver disease, Hepatology 53 (2011) 448–457.
[25] S. Huang, Y. Wu, Z. Zhao, B. Wu, K. Sun, H. Wang, L. Qin, F. Bai, Y. Leng, W. Tang, A new mechanism of obeticholic acid on NASH treatment by inhibiting NLRP3 inflammasome activation in macrophage, Metabolism 120 (2021), 154797.
[26] S. Mudaliar, R.R. Henry, A.J. Sanyal, L. Morrow, H.U. Marschall, M. Kipnes, L. Adorini, C.I. Sciacca, P. Clopton, E. Castelloe, P. Dillon, M. Pruzanski, D. Shapiro, Efficacy and safety of the farnesoid X receptor agonist obeticholic acid in patients with type 2 diabetes and nonalcoholic fatty liver disease, Gastroenterology 145 (2013), 574-82.e1.
[27] S.Y. Tian, S.M. Chen, C.X. Pan, Y. Li, FXR: structures, biology, and drug development for NASH and fibrosis diseases, Acta Pharmacol. Sin. (2022), https://doi.org/10.1038/s41401-021-00849-4.
[28] N. Stefan, H.U. Häring, K. Cusi, Non-alcoholic fatty liver disease: causes, diagnosis, cardiometabolic consequences, and treatment strategies, Lancet Diabetes Endocrinol. 7 (2019) 313–324.
[29] R. Pencek, T. Marmon, J.D. Roth, A. Liberman, R. Hooshmand-Rad, M.A. Young, Effects of obeticholic acid on lipoprotein metabolism in healthy volunteers, Diabetes Obes. Metabol. 18 (2016) 936–940.
[30] B.A. Neuschwander-Tetri, R. Loomba, A.J. Sanyal, J.E. Lavine, M.L. Van Natta, M. F. Abdelmalek, N. Chalasani, S. Dasarathy, A.M. Diehl, B. Hameed, K.V. Kowdley,

A. McCullough, N. Terrault, J.M. Clark, J. Tonascia, E.M. Brunt, D.E. Kleiner, E. Doo, Farnesoid X nuclear receptor ligand obeticholic acid for non-cirrhotic, non-alcoholic steatohepatitis (FLINT): a multicentre, randomised, placebo-controlled trial, Lancet 385 (2015) 956–965.
[31] G. Musso, M. Cassader, R. Gambino, Non-alcoholic steatohepatitis: emerging molecular targets and therapeutic strategies, Nat. Rev. Drug Discov. 15 (2016) 249–274.
[32] M. Grohmann, F. Wiede, G.T. Dodd, E.N. Gurzov, G.J. Ooi, T. Butt, A.A. Rasmiena, S. Kaur, T. Gulati, P.K. Goh, A.E. Treloar, S. Archer, W.A. Brown, M. Muller, M. J. Watt, O. Ohara, C.A. McLean, T. Tiganis, Obesity drives STAT-1-dependent NASH and STAT-3-dependent HCC, Cell 175 (2018) 1289–1306, e20.
[33] W.C. Li, S.X. Zhao, W.G. Ren, Y.G. Zhang, R.Q. Wang, L.B. Kong, Q.S. Zhang, Y. M. Nan, Co-administration of obeticholic acid and simvastatin protects against high-fat diet-induced non-alcoholic steatohepatitis in mice, Exp. Ther. Med. 22 (2021) 830.
[34] H. Jouihan, S. Will, S. Guionaud, M.L. Boland, S. Oldham, P. Ravn, A. Celeste, J. L. Trevaskis, Superior reductions in hepatic steatosis and fibrosis with co-administration of a glucagon-like peptide-1 receptor agonist and obeticholic acid in mice, Mol. Metabol. 6 (2017) 1360–1370.
[35] F. Briand, E. Brousseau, M. Quinsat, R. Burcelin, T. Sulpice, Obeticholic acid raises LDL-cholesterol and reduces HDL-cholesterol in the Diet-Induced NASH (DIN) hamster model, Eur. J. Pharmacol. 818 (2018) 449–456.
[36] J. Zhou, S. Cui, Q. He, Y. Guo, X. Pan, P. Zhang, N. Huang, C. Ge, G. Wang, F. J. Gonzalez, H. Wang, H. Hao, SUMOylation inhibitors synergize with FXR agonists in combating liver fibrosis, Nat. Commun. 11 (2020) 240.
[37] A. Ghallab, R. Hassan, U. Hofmann, A. Friebel, Z. Hobloss, L. Brackhagen, B. Begher-Tibbe, M. Myllys, J. Reinders, N. Overbeck, S. Sezgin, S. Zühlke, A. L. Seddek, W. Murad, T. Brecklinghaus, F. Kappenberg, J. Rahnenführer, D. González, C. Goldring, I.M. Copple, R. Marchan, T. Longerich, M. Vucur, T. Luedde, S. Urban, A. Canbay, T. Schreiter, M. Trauner, J.Y. Akakpo, M. Olyaee, S.C. Curry, J.P. Sowa, H. Jaeschke, S. Hoehme, J.G. Hengstler, Interruption of bile acid uptake by hepatocytes after acetaminophen overdose ameliorates hepatotoxicity, J. Hepatol. (2022), https://doi.org/10.1016/j.jhep.2022.01.020.
[38] D.M. Booth, J.A. Murphy, R. Mukherjee, M. Awais, J.P. Neoptolemos, O. V. Gerasimenko, A.V. Tepikin, O.H. Petersen, R. Sutton, D.N. Criddle, Reactive oxygen species induced by bile acid induce apoptosis and protect against necrosis in pancreatic acinar cells, Gastroenterology 140 (2011) 2116–2125.
[39] A. Abu-Shanab, E.M. Quigley, The role of the gut microbiota in nonalcoholic fatty liver disease, Nat. Rev. Gastroenterol. Hepatol. 7 (2010) 691–701.
[40] R.M. Jones, A.S. Neish, Redox signaling mediated by the gut microbiota, Free Radic. Biol. Med. 105 (2017) 41–47.
[41] A. Borrelli, P. Bonelli, F.M. Tuccillo, I.D. Goldfine, J.L. Evans, F.M. Buonaguro, A. Mancini, Role of gut microbiota and oxidative stress in the progression of non-alcoholic fatty liver disease to hepatocarcinoma: current and innovative therapeutic approaches, Redox Biol. 15 (2018) 467–479.
[42] B.L. Clifford, L.R. Sedgeman, K.J. Williams, P. Morand, A. Cheng, K.E. Jarrett, A. P. Chan, M.C. Brearley-Sholto, A. Wahlström, J.W. Ashby, W. Barshop, J. Wohlschlegel, A.C. Calkin, Y. Liu, A. Thorell, P.J. Meikle, B.G. Drew, J.J. Mack, H.U. Marschall, E.J. Tarling, P.A. Edwards, T.Q. de Aguiar Vallim, FXR activation protects against NAFLD via bile-acid-dependent reductions in lipid absorption, Cell Metabol. 33 (2021) 1671–1684, e4.
[43] G. Musso, M. Cassader, E. Paschetta, R. Gambino, Bioactive lipid species and metabolic pathways in progression and resolution of nonalcoholic steatohepatitis, Gastroenterology 155 (2018) 282–302, e8.
[44] Custers, E.M. Emma, Amanda J. Kiliaan, Dietary lipids from body to brain, Prog. Lipid Res. 85 (2022), 101144.
[45] E. Dierge, E. Debock, C. Guilbaud, C. Corbet, E. Mignolet, L. Mignard, E. Bastien, C. Dessy, Y. Larondelle, O. Feron, Peroxidation of n-3 and n-6 polyunsaturated fatty acids in the acidic tumor environment leads to ferroptosis-mediated anticancer effects, Cell Metabol. 33 (2021) 1701–1715, e5.
[46] J. Schwärzler, L. Mayr, A. Vich Vila, F. Grabherr, L. Niederreiter, M. Philipp, C. Grander, M. Meyer, A. Jukic, S. Tröger, B. Enrich, N. Przysiecki, M. Tschurtschenthaler, F. Sommer, I. Kronberger, J. Koch, R. Hilbe, M.W. Hess, G. Oberhuber, S. Sprung, Q. Ran, R. Koch, M. Effenberger, N.C. Kaneider, V. Wieser, M.A. Keller, R.K. Weersma, K. Aden, P. Rosenstiel, R.S. Blumberg, A. Kaser, H. Tilg, T.E. Adolph, PUFA-induced metabolic enteritis as a fuel for crohn's disease, Gastroenterology (2022), https://doi.org/10.1053/j.gastro.2022.01.004.
[47] Y. Rotman, A.J. Sanyal, Current and upcoming pharmacotherapy for non-alcoholic fatty liver disease, Gut 66 (2017) 180–190.
[48] C.P. Baines, R.A. Kaiser, N.H. Purcell, N.S. Blair, H. Osinska, M.A. Hambleton, E. W. Brunskill, M.R. Sayen, R.A. Gottlieb, G.W. Dorn, J. Robbins, J.D. Molkentin, Loss of cyclophilin D reveals a critical role for mitochondrial permeability transition in cell death, Nature 434 (2005) 658–662.
[49] X.X. Wang, D. Wang, Y. Luo, K. Myakala, E. Dobrinskikh, A.Z. Rosenberg, J. Levi, J. B. Kopp, A. Field, A. Hill, S. Lucia, L. Qiu, T. Jiang, Y. Peng, D. Orlicky, G. Garcia, M. Herman-Edelstein, V. D'Agati, K. Henriksen, L. Adorini, M. Pruzanski, C. Xie, K. W. Krausz, F.J. Gonzalez, S. Ranjit, A. Dvornikov, E. Gratton, M. Levi, FXR/TGR5 dual agonist prevents progression of nephropathy in diabetes and obesity, J. Am. Soc. Nephrol. 29 (2018) 118–137.
[50] X.X. Wang, T. Jiang, Y. Shen, Y. Caldas, S. Miyazaki-Anzai, H. Santamaria, C. Urbanek, N. Solis, P. Scherzer, L. Lewis, F.J. Gonzalez, L. Adorini, M. Pruzanski, J.B. Kopp, J.W. Verlander, M. Levi, Diabetic nephropathy is accelerated by farnesoid X receptor deficiency and inhibited by farnesoid X receptor activation in a type 1 diabetes model, Diabetes 59 (2010) 2916–2927.
[51] W. Jia, G. Xie, W. Jia, Bile acid-microbiota crosstalk in gastrointestinal inflammation and carcinogenesis, Nat. Rev. Gastroenterol. Hepatol. 15 (2018) 111–128.
[52] J. Liu, Y. Wei, W. Jia, C. Can, R. Wang, X. Yang, C. Gu, F. Liu, C. Ji, D. Ma, Chenodeoxycholic acid suppresses AML progression through promoting lipid peroxidation via ROS/p38 MAPK/DGAT1 pathway and inhibiting M2 macrophage polarization, Redox Biol. 56 (2022), 102452.
[53] D. Lee, J.S. Park, D. Kim, H.S. Hong, Substance P hinders bile acid-induced hepatocellular injury by modulating oxidative stress and inflammation, Antioxidants 11 (2022).
[54] F. Bäckhed, H. Ding, T. Wang, L.V. Hooper, G.Y. Koh, A. Nagy, C.F. Semenkovich, J.I. Gordon, The gut microbiota as an environmental factor that regulates fat storage, Proc. Natl. Acad. Sci. U. S. A. 101 (2004) 15718–15723.
[55] Z. Song, Y. Cai, X. Lao, X. Wang, X. Lin, Y. Cui, P.K. Kalavagunta, J. Liao, L. Jin, J. Shang, J. Li, Taxonomic profiling and populational patterns of bacterial bile salt hydrolase (BSH) genes based on worldwide human gut microbiome, Microbiome 7 (2019) 9.
[56] P. Szczepanowski, M. Noszka, D. Żyła-Uklejewicz, F. Pikuła, M. Nowaczyk-Cieszewska, A. Krężel, K. Stingl, A. Zawilak-Pawlik, HP1021 is a redox switch protein identified in Helicobacter pylori, Nucleic Acids Res. 49 (2021) 6863–6879.
[57] A. Di Sessa, S. Riccio, E. Pirozzi, M. Verde, A.P. Passaro, G.R. Umano, S. Guarino, E. Miraglia Del Giudice, P. Marzuillo, Advances in paediatric nonalcoholic fatty liver disease: role of lipidomics, World J. Gastroenterol. 27 (2021) 3815–3824.
[58] M. Notarnicola, A.R. Osella, M.G. Caruso, P.L. Pesole, A. Lippolis, V. Tutino, C. Bonfiglio, V. De Nunzio, M.P. Scavo, A. Mirizzi, I. Franco, T. Lippolis, R. D'Alessandro, M.G. Refolo, C. Messa, Nonalcoholic fatty liver disease: focus on new biomarkers and lifestyle interventions, Int. J. Mol. Sci. 22 (2021).
[59] R.P. Bazinet, S. Layé, Polyunsaturated fatty acids and their metabolites in brain function and disease, Nat. Rev. Neurosci. 15 (2014) 771–785.
[60] X. Chen, R. Kang, G. Kroemer, D. Tang, Broadening horizons: the role of ferroptosis in cancer, Nat. Rev. Clin. Oncol. 18 (2021) 280–296.
[61] C. Corbet, E. Bastien, J.P. Santiago de Jesus, E. Dierge, R. Martherus, C. Vander Linden, B. Doix, C. Degavre, C. Guilbaud, L. Petit, C. Michiels, C. Dessy, Y. Larondelle, O. Feron, TGFβ2-induced formation of lipid droplets supports acidosis-driven EMT and the metastatic spreading of cancer cells, Nat. Commun. 11 (2020) 454.
[62] V.E. Kagan, G. Mao, F. Qu, J.P. Angeli, S. Doll, C.S. Croix, H.H. Dar, B. Liu, V. A. Tyurin, V.B. Ritov, A.A. Kapralov, A.A. Amoscato, J. Jiang, T. Anthonymuthu, D. Mohammadyani, Q. Yang, B. Proneth, J. Klein-Seetharaman, S. Watkins, I. Bahar, J. Greenberger, R.K. Mallampalli, B.R. Stockwell, Y.Y. Tyurina, M. Conrad, H. Bayır, Oxidized arachidonic and adrenic PEs navigate cells to ferroptosis, Nat. Chem. Biol. 13 (2017) 81–90.
[63] P. Puri, R.A. Baillie, M.M. Wiest, F. Mirshahi, J. Choudhury, O. Cheung, C. Sargeant, M.J. Contos, A.J. Sanyal, A lipidomic analysis of nonalcoholic fatty liver disease, Hepatology 46 (2007) 1081–1090.
[64] P. Puri, M.M. Wiest, O. Cheung, F. Mirshahi, C. Sargeant, H.K. Min, M.J. Contos, R. K. Sterling, M. Fuchs, H. Zhou, S.M. Watkins, A.J. Sanyal, The plasma lipidomic signature of nonalcoholic steatohepatitis, Hepatology 50 (2009) 1827–1838.
[65] C. López-Vicario, A. Checa, A. Urdangarin, F. Aguilar, J. Alcaraz-Quiles, P. Caraceni, A. Amorós, M. Pavesi, D. Gómez-Cabrero, J. Trebicka, K. Oettl, R. Moreau, N. Planell, V. Arroyo, C.E. Wheelock, J. Clària, Targeted lipidomics reveals extensive changes in circulating lipid mediators in patients with acutely decompensated cirrhosis, J. Hepatol. 73 (2020) 817–828.
[66] S. Wei, T. Qiu, N. Wang, X. Yao, L. Jiang, X. Jia, Y. Tao, J. Zhang, Y. Zhu, G. Yang, X. Liu, S. Liu, X. Sun, Ferroptosis mediated by the interaction between Mfn2 and IREα promotes arsenic-induced nonalcoholic steatohepatitis, Environ. Res. 188 (2020), 109824.
[67] J. Zhao, H.H. Dar, Y. Deng, C.M. St Croix, Z. Li, Y. Minami, I.H. Shrivastava, Y. Y. Tyurina, E. Etling, J.C. Rosenbaum, T. Nagasaki, J.B. Trudeau, S.C. Watkins, I. Bahar, H. Bayır, A.P. VanDemark, V.E. Kagan, S.E. Wenzel, PEBP1 acts as a rheostat between prosurvival autophagy and ferroptotic death in asthmatic epithelial cells, Proc. Natl. Acad. Sci. U. S. A. 117 (2020) 14376–14385.
[68] S. Wang, Z. Liu, J. Geng, L. Li, X. Feng, An overview of ferroptosis in non-alcoholic fatty liver disease, Biomed. Pharmacother. 153 (2022), 113374.
[69] H. Yki-Järvinen, Non-alcoholic fatty liver disease as a cause and a consequence of metabolic syndrome, Lancet Diabetes Endocrinol. 2 (2014) 901–910.
[70] C.O. Zein, R. Lopez, X. Fu, J.P. Kirwan, L.M. Yerian, A.J. McCullough, S.L. Hazen, A.E. Feldstein, Pentoxifylline decreases oxidized lipid products in nonalcoholic steatohepatitis: new evidence on the potential therapeutic mechanism, Hepatology 56 (2012) 1291–1299.
[71] C. Jiang, C. Xie, Y. Lv, J. Li, K.W. Krausz, J. Shi, C.N. Brocker, D. Desai, S.G. Amin, W.H. Bisson, Y. Liu, O. Gavrilova, A.D. Patterson, F.J. Gonzalez, Intestine-selective farnesoid X receptor inhibition improves obesity-related metabolic dysfunction, Nat. Commun. 6 (2015), 10166.
[72] W.L. Holland, S.A. Summers, Sphingolipids, insulin resistance, and metabolic disease: new insights from in vivo manipulation of sphingolipid metabolism, Endocr. Rev. 29 (2008) 381–402.
[73] N. Wasilewska, A. Bobrus-Chociej, E. Harasim-Symbor, E. Tarasów, M. Wojtkowska, A. Chabowski, D.M. Lebensztejn, Increased serum concentration of ceramides in obese children with nonalcoholic fatty liver disease, Lipids Health Dis. 17 (2018) 216.
[74] B. Guan, J. Tong, H. Hao, Z. Yang, K. Chen, H. Xu, A. Wang, Bile acid coordinates microbiota homeostasis and systemic immunometabolism in cardiometabolic diseases, Acta Pharm. Sin. B 12 (2022) 2129–2149.
[75] S. Tomioka, N. Seki, Y. Sugiura, M. Akiyama, J. Uchiyama, G. Yamaguchi, K. Yakabe, R. Ejima, K. Hattori, T. Kimizuka, Y. Fujimura, H. Sato, M. Gondo,

S. Ozaki, Y. Honme, M. Suematsu, I. Kimura, N. Inohara, G. Núñez, K. Hase, Y. G. Kim, Cooperative action of gut-microbiota-accessible carbohydrates improves host metabolic function, Cell Rep. 40 (2022), 111087.

[76] L. Demetrius, Of mice and men. When it comes to studying ageing and the means to slow it down, mice are not just small humans, EMBO Rep. 6 (2005). Spec No:S39-44.

[77] L. Sun, C. Xie, G. Wang, Y. Wu, Q. Wu, X. Wang, J. Liu, Y. Deng, J. Xia, B. Chen, S. Zhang, C. Yun, G. Lian, X. Zhang, H. Zhang, W.H. Bisson, J. Shi, X. Gao, P. Ge, C. Liu, K.W. Krausz, R.G. Nichols, J. Cai, B. Rimal, A.D. Patterson, X. Wang, F. J. Gonzalez, C. Jiang, Gut microbiota and intestinal FXR mediate the clinical benefits of metformin, Nat. Med. 24 (2018) 1919–1929.

[78] D.E. Kleiner, E.M. Brunt, M. Van Natta, C. Behling, M.J. Contos, O.W. Cummings, L. D. Ferrell, Y.C. Liu, M.S. Torbenson, A. Unalp-Arida, M. Yeh, A.J. McCullough, A. J. Sanyal, Design and validation of a histological scoring system for nonalcoholic fatty liver disease, Hepatology 41 (2005) 1313–1321.

[79] Y. Liu, K. Chen, F. Li, Z. Gu, Q. Liu, L. He, T. Shao, Q. Song, F. Zhu, L. Zhang, M. Jiang, Y. Zhou, S. Barve, X. Zhang, C.J. McClain, W. Feng, Probiotic lactobacillus rhamnosus GG prevents liver fibrosis through inhibiting hepatic bile acid synthesis and enhancing bile acid excretion in mice, Hepatology 71 (2020) 2050–2066.

[80] H. Tanaka, K. Doesburg, T. Iwasaki, I. Mierau, Screening of lactic acid bacteria for bile salt hydrolase activity, J. Dairy Sci. 82 (1999) 2530–2535.